2001-07-25

Predicting the Effects of Dimensional and Material Property Variations in Micro Compliant Mechanisms

Jonathan W. Wittwer
Brigham Young University - Provo

PREDICTING THE EFFECTS OF DIMENSIONAL AND MATERIAL PROPERTY VARIATIONS IN MICRO COMPLIANT MECHANISMS

by

Jonathan W. Wittwer

A thesis submitted to the faculty of

Brigham Young University

in partial fulfillment of the requirements for the degree of

Master of Science

Department of Mechanical Engineering

Brigham Young University

December 2001

BRIGHAM YOUNG UNIVERSITY

GRADUATE COMMITTEE APPROVAL

of a thesis submitted by

Jonathan W. Wittwer

This thesis has been read by each member of the following graduate committee and by majority vote has been found to be satisfactory.

_____	_____
Date	Larry L. Howell, Chair
_____	_____
Date	Kenneth W. Chase
_____	_____
Date	Alan R. Parkinson

BRIGHAM YOUNG UNIVERSITY

As chair of the candidate's graduate committee, I have read the thesis of Jonathan W. Wittwer in its final form and have found that (1) its format, citations, and bibliographical style are consistent and acceptable and fulfill university and department style requirements; (2) its illustrative materials including figures, tables, and charts are in place; and (3) the final manuscript is satisfactory to the graduate committee and is ready for submission to the university library.

_____ _____

Date

Larry L. Howell
Chair, Graduate Committee

Accepted for the Department

_____

Brent L. Adams
Graduate Coordinator

Accepted for the College

_____

Douglas M. Chabries
Dean, College of Engineering and Technology

ABSTRACT

PREDICTING THE EFFECTS OF DIMENSIONAL AND MATERIAL PROPERTY VARIATIONS IN COMPLIANT MECHANISMS

Jonathan W. Wittwer

Department of Mechanical Engineering

Master of Science

Surface micromachining of micro-electro-mechanical systems (MEMS), like all other fabrication processes, has inherent variation that leads to uncertain material and dimensional parameters. To obtain accurate and reliable predictions of mechanism behavior, the effects if these variations need to be analyzed. This thesis expands already existing tolerance and uncertainty analysis methods to apply to micro compliant mechanisms. For simple compliant members, explicit equations can be used in uncertainty analysis. However, for a nonlinear implicit system of equations, the direct linearization method may be used to obtain sensitivities of output parameters to small changes in known variables. This is done by including static equilibrium equations and pseudo-rigid-body model relationships with the kinematic vector loop equations. Examples are used to show a comparison of this method to other deterministic and probabilistic methods and finite element analysis.

ACKNOWLEDGMENTS

This thesis is based upon work supported under a National Science Foundation Graduate Research Fellowship. The author would also like to acknowledge the support of his family, committee members, and fellow research assistants.

TABLE OF CONTENTS

LIST OF TABLES

LIST OF FIGURES

CHAPTER 1

INTRODUCTION

1.1 Purpose

In micro-electro-mechanical systems (MEMS), assembly is very difficult due to the size of the mechanisms, so other methods are used to create self-assembled mechanisms. However, variations in the fabrication process lead to uncertain dimensions. At the micro scale, where precision and reliability are very important, the effects of these variations need to be considered.

Compliant mechanisms, mechanisms that gain some or all of the motion from the deflection of members, often have the unique ability to be fabricated without the need for assembly, and thus are gaining popularity in MEMS. Although compliance can eliminate clearance in joints and the associated errors, compliant mechanisms have unique characteristics that make them sensitive to certain variations. The purpose of this thesis is to develop a method for analyzing the effects of dimensional and material property variations on the mechanical error in compliant mechanisms, and demonstrate its use through case studies in MEMS. Some of the specific questions to be answered are listed below:

- How do variations in the dimensional and material parameters affect the forces and coupler position of a compliant mechanism?
- What methods can be used to determine the mechanical error in compliant mechanisms with nonlinear deflections?

Preliminary research has led to the following hypotheses that will be tested:

- For simple compliant mechanisms that can be reduced to the deflection of a cantilever beam, large-deflection equations can be linearized in order to perform a complete error analysis considering uncertainty in both dimensional and material parameters.
- The direct linearization method and the use of the pseudo-rigid-body model make it possible to determine the sensitivity of compliant mechanisms to variations in dimensional and material parameters.

1.2 Delimitation

Micro-electro-mechanical systems are generally planar in nature, hence the mechanism analysis methods applied herein will be restricted to two dimensions. Although clearances in joints contribute to mechanical error, only dimensional variations will be considered. Although the methods described could possibly be used in mechanism synthesis, they will only be applied to post-synthesis error analysis. Since mechanism synthesis is not considered, the error associated with the mechanism analysis will not include structural error. The analysis is based upon given tolerances or variation; therefore, no work

will be discussed pertaining to the trade-off between cost of manufacturing and mechanical error. Although some analysis will involve forces, dynamic effects of clearances and tolerances will not be discussed.

1.3 Outline

The next chapter will review the work that has been done in compliant mechanisms, micro-electro-mechanical systems, and mechanical error analysis. It will also define the types of variations common to micro-electro-mechanical systems. In Chapter 3, the simplification of large-deflection cantilever beam equations will be used to demonstrate how to calculate the sensitivities of parameter variations for flexible members using explicit equations. This discussion will also validate the need for performing error analysis in MEMS. Chapter 4 will compare deterministic and probabilistic methods for determining the mechanical error in kinematic linkages. Here, the direct linearization method will be outlined and the bivariate nature of position error in assemblies will be discussed. In Chapter 5, the direct linearization method will be used to analyze the mechanical error in compliant mechanisms by including force-equilibrium equations and pseudo-rigid-body model relationships. Finally, the conclusions drawn from this research will be summarized and recommendations will be made for further research.

CHAPTER 2 BACKGROUND

This chapter gives the background to compliant mechanisms, micro-electro-mechanical systems (MEMS), and mechanical error in linkages. It contains a review of the literature pertaining to mechanical error in compliant mechanisms and MEMS, and brief reviews of the history of the three subjects.

2.1 Compliant Mechanisms

2.1.1 Definition

Compliant mechanisms, or flexible link mechanisms, gain some or all of their motion through the deflection of flexible members (Sevak and McLarnan, 1974). A fully compliant mechanism is one that has no rigid body joints. A partially compliant mechanism is one that has some compliant members and some non-compliant joints (e.g. a passive revolute joint).

2.1.2 History

One of the earliest compliant mechanisms used by mankind is the bow, but Mother Nature has used compliance since the beginnings of life in things such as plants and the wings and legs of small insects. The ability of mankind to synthesize the design of compliant mechanism has only existed a short time.

Euler was the first to quantify the deflection of flexible beams with the development of the Bernoulli-Euler equation. In 1945, Bisshopp and Drucker used elliptic integral solutions to describe large deflection of cantilever beams. These solutions have very limited applications and are difficult to use. Since then, semi-graphical methods (Burns and Crossley, 1966; Burns and Crossley, 1968), finite-element methods (Sevak and McLarnan, 1974; Gandhi, 1981), topology optimization methods (Ananthasuresh et al., 1993; Frecker et al., 1996, 1997, 1998), pseudo-rigid-body methods (Howell and Midha, 1994b, 1995a), and various other methods (Gorski, 1976) have been developed to analyze and synthesize compliant mechanisms at both the macro and micro scales.

2.1.3 The Pseudo-Rigid-Body Model

Although there are many methods for analyzing compliant mechanisms, one of the simplest is the use of the pseudo-rigid-body model (PRBM), which has gained popularity due to the ability to use conventional kinematic analysis. This method involves replacing flexible segments with rigid links that have pin joints with torsional springs. Not all flexible segments can be analyzed using this method, but a large number of typical configura-

tions have been analyzed. These are listed in Table 2.1, along with the reference in which a more detailed description can be found.

By combining the models for the particular beam deflections and using the symmetry of certain segments, these models can be applied to a surprisingly large number of configurations. The process of synthesizing mechanisms using the PRBM has been described in detail by Howell and Midha (1996a).

The Pseudo-Rigid-Body Model is an approximation, so when calculating mechanical error, the error within in the model itself must be realized. In general, the position or deflection errors associated with the PRBM increase with increasing deflection. The maximum deflections for the PRBMs have been determined by Howell and Midha (1995b) for keeping this error under 0.5%.

A detailed description of the PRBM will not be discussed herein. The reader is referred to the references listed in Table 2.1. The model has proven to be very useful in design and analysis of compliant mechanisms (Derderian et al., 1996; Derderian, 1996; Howell et al., 1994c; Howell and Midha, 1995b; Howell and Midha, 1996a; Jensen et al.,

TABLE 2.1 PRBM configurations and associated references.

PRBM Configurations	**Reference**
Small Length Flexural Pivots	(Howell and Midha, 1994a)
End-Loaded Cantilever Beams	(Howell and Midha, 1995a)
Fixed-Guided Flexible Segments	(Howell et al., 1996)
End-Loaded Initially Curved Cantilever Beams	(Howell and Midha, 1996b)
Functionally Binary Pinned-Pinned Segment	(Edwards et al., 1999)
Moment and End-Loaded Cantilever Beams	(Lyon et al. 2000)

1997; Jensen et al., 1998; Lyon et al., 1997; Mettlach and Midha, 1996; Millar et al., 1996; Opdahl, 1996; Opdahl et al., 1998; Salmon et al., 1996).

2.2 MEMS

2.2.1 Definition and Fabrication

Micro-electro-mechanical systems (MEMS) integrate electrical circuitry with mechanical devices having dimensions measured in microns. Although there are many processes used to create MEMS, these devices are typically manufactured using surface micro-machining. Although there are a wide variety of surface micro-machining methods and materials, the processes associated with the Multi-User MEMS Process (MUMPs™) will be detailed in this thesis. This process includes an insulating silicon nitride layer, three layers of polycrystalline silicon (polysilicon), two layers of phosphosilicate glass (PSG), and a gold metal layer.

In short, surface micro-machining of MEMS on silicon wafers involves a combination of thin film depositions, patterning, and etching, followed by a release process, to form planar structures. The polysilicon layers are structural, while the PSG layers are sacrificial - meaning that they are deposited only as a means of separating other layers. These sacrificial layers are chemically etched (using hydrofluoric acid) to release the moving or suspended parts. The metal layer is used for electrical circuitry and contacts.

The many limitations associated with surface micro-machining make designing micro mechanisms complex. Some of the complications of MEMS design include scaling

material properties, adhesion forces, stiction, dimensional constraints, self-assembly, and limited motion.

2.2.2 History

The design of MEMS is only a fairly recent development, having its beginnings in the early 1980s. The development of advanced integrated circuit processes has enabled engineers to take advantage of silicon's excellent combination of electrical and mechanical properties. The first major applications for MEMS were micro sensors that are now being used in everything from accelerometers that trigger air bags to scuba-diving equipment (Bryzek et al., 1994; Wise, 1991). As predicted, research in MEMS has become an inter-disciplinary field that includes mechanical, electrical, chemical, and biomedical fields (Komvopoulos, 1998). Fujita (1997) provides an excellent overview of the history and future of MEMS. Kota et al. (1994) summarizes many of the challenges of designing micro mechanisms from a mechanical engineering perspective.

2.2.3 Use of Compliance in MEMS

Compliant mechanisms are often well suited for MEMS applications. Many of the difficulties associated with MEMS can be overcome by using compliance, such as elimination of wear, lubrication, friction, and clearance problems associated with the pin joints. In addition, compliant mechanisms are planar in nature, do not require assembly, and can be made using a single layer. The work done by Clements (1999) provides an overview of how compliant mechanisms can be implemented in MEMS.

2.2.4 Material Properties of Silicon

The main structural material for use in surface micro-machined MEMS is polycrystalline silicon. Although the bulk material properties of silicon are well known (Petersen, 1982), the properties of polysilicon, especially scaled down to micro dimensions are not well defined. It is not within the scope of this thesis to discuss in detail the properties of silicon and polysilicon, but rather to determine how uncertainties in material properties can lead to mechanical error. A good description of the how the material properties of silicon affect compliant mechanism design is provided by Opdahl (1996).

Although the electrical and thermal properties of silicon and polysilicon are well known (because of their extensive use in integrated circuits), the mechanical properties are not well understood. Work is being done to get more exact measurements for important mechanical characteristics of polysilicon, such as Young's modulus and strength. Sharpe and Jackson (2000) have determined that Young's modulus for polysilicon is 160 ± 10 GPa. Even though the uncertainty is fairly large (±6%), they propose that this variation is not critical because it is much more precise than the present ability to measure the cross-sectional area of a MEMS device. This assumption is one that will be investigated in this thesis, since compliant mechanisms are highly dependent on the value of Young's modulus.

One of the complications of using polysilicon as a structural material is the relative size of the grains with respect to the overall size of the mechanism. The size of the grains vary with each batch of deposited polysilicon, but can be on the order of 0.5 microns.

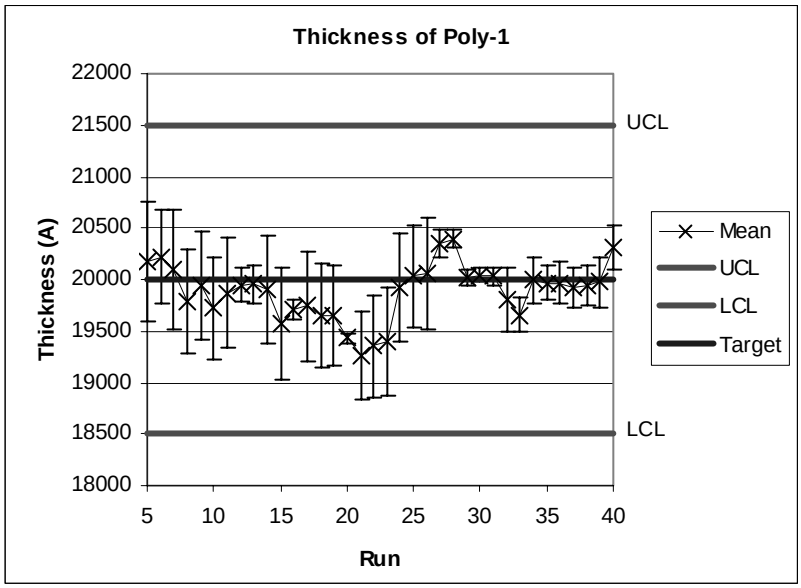

Figure 2.1 Poly-1 layer thickness over 35 MUMPs™ runs.

Sharpe et al. (1997) found that for the MUMPs™ process, the grains are generally columnar and oriented perpendicular to the substrate. The presence of the grain boundaries, which are typically about 0.5-1.0 nm wide, have many effects on the material properties (Wolf and Tauber, 2000). They lead to larger variations in the structural properties and change the thermal and electrical properties.

2.2.5 Dimensional Variations

Thickness Variation:

Both the polysilicon and the sacrificial PSG layers are grown using low pressure chemical vapor deposition (LPCVD). This is a timed process designed to produce a nominal thickness for each layer. The process control chart shown in Figure 2.1 shows the variation in the thickness of the first polysilicon film for the first 35 MUMPs™ runs, where the error bars represent plus and minus one standard deviation from the mean.

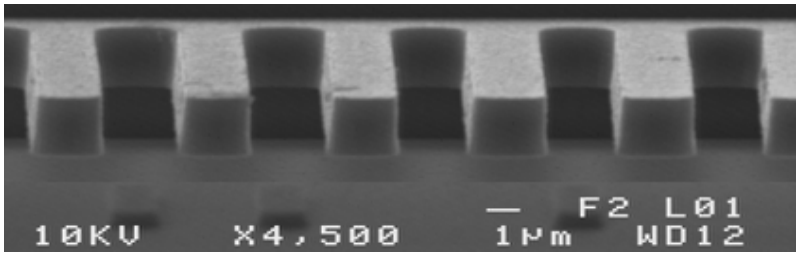

Figure 2.2 End of a polysilicon cantilever beam.

Although the standard deviation for each individual run is small (approximately 200 angstroms for the latest runs), the mean shifts from run to run, so when predicting the thickness of the layer, upper and lower control limits (UCL and LCL) or tolerances have been set to represent the minimum and maximum thicknesses. Table 2.2, adapted from the MUMPs™ Design Handbook (Koester et al., 2000), lists these minimum and maximum thicknesses for each layer, along with the nominal value. The standard deviation for thickness, when predicting the mean for future runs, is approximately one third of the tolerance.

Width Variation:

The geometry in the various polysilicon and PSG layers is created using a Reactive Ion Etch (RIE). Although the masks can be made very precise, the variables in the etch process lead to variations in the smoothness and angle of the side-walls (Mirfendereski et al., 1993). Figure 2.2 shows a scanning electron micrograph of the end of a poly-

TABLE 2.2 Thicknesses of deposited films in MUMPs™.

	Thickness in (μm)		
Film	**Min.**	**Typ.**	**Max.**
Nitride	0.530	0.600	0.670
Poly0	0.470	0.500	0.530
Oxide1	1.750	2.000	2.250
Poly1	1.850	2.000	2.150
Oxide2	0.670	0.750	0.830
Poly2	1.400	1.500	1.600
Metal	0.460	0.520	0.580

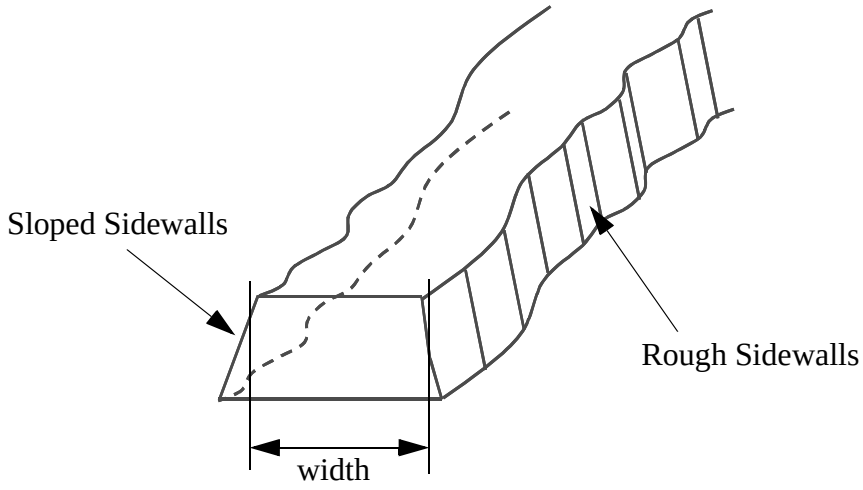

Figure 2.3 Width variation due to sidewall slope and roughness.

silicon cantilever beam designed to be 2 microns thick and 3 microns wide. Note that the side-walls are not perfectly vertical. Figure 2.3 shows an exaggerated diagram of how sidewall roughness and slope contribute to width variation.

2.2.6 Mechanical Error in MEMS

Little work has been done to model mechanical error in micro mechanisms due to material property and dimensional variations; however, compliant mechanisms are known to be particularly sensitive to Young's modulus and cross-sectional dimensions. Therefore, the design of reliable MEMS must take into account both the uncertainties associated with material properties and variations in the fabrication process, especially since the uncertainties and variations are large in comparison to the nominals.

2.3 Mechanical Error

2.3.1 Error Definitions

Mechanisms are often designed for function, path, or motion generation. Function generation relates the orientation of an output link to the orientation of an input link. Path generation describes the location of a coupler point through space. Motion generation describes both the path and orientation of the coupler. The kinematic function of a mechanism is a more general term that can include any or all of these. Joskowicz et al. (1997) defined the kinematic function of a mechanism as "...the relationship among the motions of its parts imposed by contacts between them." An example of a kinematic function for a compliant MEMS might be the position of a point on a coupler link for a given displacement of a thermally expanded member.

The kinematic error of a mechanism can be divided into two main categories, structural (mathematical) error and mechanical error (Hartenberg and Denavit, 1964). Structural error is that associated with mechanism synthesis when a specific kinematic function is desired and the mechanism cannot achieve the function exactly, even when the dimensions are exact. Mechanical error is associated with variations in manufacturing processes and dynamic effects, in addition to dimensional variations. Some of the sources of mechanical error in rigid linkages are link flexibility, axial deflection, lateral deflection, torsional deflection, and joint clearances. Joint clearances are usually the largest cause of mechanical error (Vocaturo, 1983). Coit and Riley classify the three main error sources as link length tolerances, joint clearances, and link static and dynamic deflections (Coit and

Riley, 1981). Rigid linkages are usually designed so that the link deflections can be neglected, so only the link length tolerances and joint clearances are considered; whereas, compliant mechanisms are designed to deflect, so they are more subject to variations in the height and width of the links. Therefore, even though compliant joints eliminate one of the largest sources of error (joint clearances), additional sources of error are added due to the flexibility of the segment.

Note: In this thesis, in order to characterize the mechanical error, the structural error will not be considered, or it will be considered to be zero. The ideal kinematic function will be based upon expected values for link dimensions and no clearance in joints. The structural error would be the deviation of the ideal kinematic function from another predefined function. Treating the structural error as zero means that the mechanical error will be the deviation from the ideal kinematic function.

2.3.2 Dimensional Tolerances vs. Joint Clearances

Care must be taken in comparing the sources of mechanical error. Tolerances on dimensions based upon the inadequacies of manufacturing processes to produce exact sizes have a different effect on the mechanical error than do joint clearances. Dimensional tolerances can be analyzed using statistical models because tolerances, by nature, are statistical. For example, when designing a part to be 5.00 cm long, the process used to make the part may only be able to achieve that dimension to within ±0.03 cm. This is usually interpreted to mean that the expected part dimension will be 5.00 cm with a standard deviation of 0.01 cm (one third of the tolerance).

In contrast, the clearance in a joint is based upon the combination of two tolerances (the variation in diameters of the pin and hole). The resulting complexity in analysis comes in trying to determine how to model the shift in the relative axial position of pin and hole. Although this thesis does not include joint clearances in the analysis of mechanical error, it provides a basis for further research in that area.

2.3.3 Previous Research in Mechanical Error

The problem of mechanical error was addressed in the 19th century when a mathematician, Charles Babbage, tried to make a mechanical computer. It failed because of the accumulation of errors from tolerances and joint clearances (Morrisson and Morrisson, 1961). One of the first detailed investigations of the effects of tolerances on mechanical error in mechanisms was made by Knappe (1963). His approach was based upon the random nature of tolerances, and by using probabilistic methods, was able to find sensitivity coefficients relating the amount of error due to individual variables. Hartenberg and Denavit (1964) were among the first to include mechanical error analysis in a textbook. Like Knappe however, their analysis was limited to just link length tolerances. Since these early studies, many methods for determining the static and dynamic effects of tolerances and clearances on mechanical error have been developed.

Extending the methods of Knappe (1963), Garrett and Hall (1969) developed a statistical approach to determine mechanical error due to both tolerances and clearances and represented the error as mobility bands. Schade (1983) used a bivariate normal model to determine the position error of a coupler point. He concluded that the root mean square

approach for position error is much too conservative. The work by Choi et al. (1998) shows various improved stochastic methods applied to mechanical error including both link length tolerances and clearances.

An interesting aspect of research in mechanical error is the presence of a parallel body of literature that branches from a different origin, but is now paralleling the studies already cited. Chase and Parkinson (1991) provide a survey of research in tolerance analysis of mechanical assemblies. This field originates from the need for tolerance analysis in design for manufacture, where most of the models are static assemblies. However, the methods used to analyze static assemblies have also been to kinematic mechanisms. The main link between the two communities is the use of vector loops to describe assemblies and kinematic linkages. An effective method used in assembly tolerance analysis, called the Direct Linearization Method (Marler, 1988; Chase et al., 1995), is based upon the linearization of a system of vector loop equations. This is the method which will be extended in this thesis to analyze compliant mechanisms.

2.3.4 Deterministic vs. Probabilistic Methods:

The many methods for analyzing the effects of tolerances in mechanisms can be placed into two different groups: deterministic and probabilistic. Deterministic methods involve fixed values or constraints that are used to find a single exact solution. Deterministic methods are used mostly for post-synthesis analysis, where set tolerances are used to determine worst-case position error.

In contrast, probabilistic or statistical methods involve random variables that result in a probabilistic response, which predicts the range of possible solutions. In addition to analysis, statistical methods may be used for analyzing or optimizing tolerances during mechanism synthesis, where the dimensions have some type of probability distribution associated with them.

Chapter 4 will compare various deterministic and probabilistic methods as a means of validating the direct linearization method.

2.3.5 Spatial / Matrix Methods:

Due to the special interest in robotics to determine the effects of joint clearances, many matrix methods have been used to determine the effects of joint clearances. Generally, a transformation matrix is defined to describe the relative displacement between pin and bearing (Kinzel and Hall, 1975; Waldron and Kumar, 1979). Both deterministic and stochastic models have been based upon transformation matrices. Zhu and Ting (2000) developed the probability distribution function for a robotic manipulator based upon both normal and uniform distributions. This enables them to determine the uncertainty in position for the end-point of the manipulator, but only works for open-loop kinematic chains.

2.3.6 Computer Simulations / Optimization:

The use of computers has spawned many methods for analyzing mechanisms. Monte Carlo simulations have been used to validate statistical models (Choi et al., 1998; Shi, 1997; Lee and Gilmore, 1991; Wei-Liang and Qi-Xian, 1989), but even with modern computing power, Monte Carlo simulations are often too computationally expensive.

Other approaches may use optimization for determining the trade-off between manufacturing costs and errors due to tolerances (Rhyu and Kwak, 1988; Biswas and Kinzel, 1998c). In addition, optimization methods offer a way to analyze very complex mechanisms involving many variables and constraints. Schade and Lai (1983) developed a technique in which nonlinear optimization was used to determine the maximum error in coupler-point position due to pin-joint clearances and link tolerances. The path-normal error for a straight-line mechanism was determined using this technique. Yin and Wu (1990) used a very similar approach, but included some dynamic analysis in their method to get a quasi-static model.

Another method that has been made possible by the use of computers is stochastic finite element analysis, which is currently one of the only methods for determining the probabilistic response of compliant mechanisms. Mirfendereski et al. (1993) has applied this method to analyze uncertainty in micro strain gauges.

Joskowicz and Sacks (1997) have produced a computer program for analyzing the kinematic tolerance space of mechanisms by reducing the tolerance analysis to computational geometry. Although it works for determining variations in the kinematic function of rigid linkages, it does not account for large non-linear deflections typical of compliant mechanisms.

New computer software for analyzing effects of tolerances continues to be developed as more importance is placed on using computer simulations in product development. Early software could only be applied to specific applications, but with the

development of more general analysis methods, the scope of the software can be expanded. For example, the Pseudo-Rigid-Body Model allows compliant mechanisms to be analyzed using normal kinematic analysis tools. Likewise, new methods of variation analysis that can circumvent the need for Monte Carlo simulations or Finite Element analysis, may prove to be useful in mechanism synthesis.

2.3.7 Dimensional Variations in Compliant MEMS:

Only a few people have looked at the effects of dimensional variations on the design of micro mechanisms. Mirfendereski et al. (1993) applied stochastic finite element methods to analyze uncertainty in micro strain gauges. Howell et al. (1994d) included variation in link lengths, material properties, and cross-sectional dimensions in the analysis of the reliability of a bistable compliant mechanism, but did not consider force or position error.

2.4 Summary

Much work has been done to determine the effects of tolerances on mechanical error in rigid mechanisms and assemblies. As explained in Section 2.3.1, compliant mechanism analysis contains additional complications that require further study. In addition to link length variations, compliant mechanisms may be sensitive to cross-sectional dimensions in flexible members, reaction forces, and material properties. For micro compliant mechanisms, these additional variations may prove to be very significant.

CHAPTER 3

UNCERTAINTY IN COMPLIANT MEMBERS

This chapter discusses the theory of uncertainty analysis and demonstrates how it is applied to explicit equations with random variables. It is important to determine the effects of dimensional variations and material property uncertainty on the forces and stresses in compliant members. To do this, a vertically end-loaded cantilever beam will be analyzed. For large deflections, the equations are nonlinear and none explicit. However, this chapter will demonstrate a method of obtaining an explicit equation that can be used even for large deflections.

3.1 Uncertainty Analysis

Given a function $f(\psi_1, \psi_2, \ldots, \psi_i)$, where $\psi_1, \psi_2, \ldots, \psi_i$ are independent random variables with standard deviations of $\sigma_1, \sigma_2, \ldots, \sigma_i$, respectively, the approximate variance of f is calculated as:

$$\sigma_f^2 = \left(\frac{\partial f}{\partial \psi_1}\right)^2 \sigma_1^2 + \left(\frac{\partial f}{\partial \psi_2}\right)^2 \sigma_2^2 + \ldots + \left(\frac{\partial f}{\partial \psi_i}\right)^2 \sigma_i^2 \tag{3.1}$$

where the partial derivatives are calculated using the expected (mean) values. The partial derivatives are the sensitivities of the function with respect to changes in the random variables, whereas the individual terms are the variance components. The variance components are often represented as a percentage of the total variance in order to determine the relative contribution of each of the variables. Equation (3.1) is an accurate approximation if the function is well-behaved (not highly nonlinear) and if the variations are relatively small ($\sigma_i << \psi_i$). For the purposes of this thesis, all random variables will be assumed to be normally distributed.

As an example, consider the explicit equation relating the force of a vertically end-loaded cantilever to the vertical deflection at the end of the beam:

$$P = \frac{3EI\delta}{L^3} = \frac{Ewh^3\delta}{4L^3} \tag{3.2}$$

where the moment of inertia, *I*, for a rectangular beam is $(wh^3)/12$, *P* is the force, δ is the beam deflection, *w* is the width of the beam, *h* is the height, *L* is the length, and *E* is Young's modulus. Of course, this assumes the beam deflection is small and that the beam is linearly elastic, isotropic, and homogeneous.

The force variance of the beam is found by applying Equation (3.1) as follows:

$$\sigma_P^2 = \left(\frac{\partial P}{\partial E}\right)^2 \sigma_E{}^2 + \left(\frac{\partial P}{\partial w}\right)^2 \sigma_w{}^2 + \left(\frac{\partial P}{\partial h}\right)^2 \sigma_h{}^2 + \left(\frac{\partial P}{\partial L}\right)^2 \sigma_L{}^2 + \left(\frac{\partial P}{\partial \delta}\right)^2 \sigma_\delta{}^2 = \tag{3.3}$$

$$\left(\frac{wh^3\delta}{4L^3}\right)^2 \sigma_E{}^2 + \left(\frac{Eh^3\delta}{4L^3}\right)^2 \sigma_w{}^2 + \left(\frac{3Ewh^2\delta}{4L^3}\right)^2 \sigma_h{}^2 + \left(-\frac{3Ewh^3\delta}{4L^4}\right)^2 \sigma_L{}^2 + \left(\frac{Ewh^3}{4L^3}\right)^2 \sigma_\delta{}^2$$

This analysis is limited to small beam deflections, but most compliant mechanisms operate in the nonlinear (large deflection) range. The following section will demonstrate a method for simplifying the force-deflection relationship for nonlinear deflections so that this same method of uncertainty analysis can be applied.

3.2 Simplifying the Non-Linear Force-Deflection Relationship

3.2.1 Elliptic Integral Solution

Bisshop and Drucker (1945) developed a closed-form elliptic integral solution for the large deflection of end-loaded cantilever beams. This solution is based upon the Bernoulli-Euler equation which states that the moment in the beam is directly proportional to its curvature. A comparison of the elliptic integral solution to equation (3.2) shows that error is a function of the ratio δ/L (beam deflection / beam length). The percent error is defined to be $(P - P_{elliptic})/P_{elliptic}$, where P is the force found from equation (3.2). By curve fitting the percent error to the ratio δ/L (Figure 3.1), equation (3.2) can be modified to give a simplified explicit equation that gives the nominal force for a given beam deflection:

$$P = \frac{Ewh^3\delta}{4L^3}\frac{1}{1+\varepsilon_P} \tag{3.4}$$

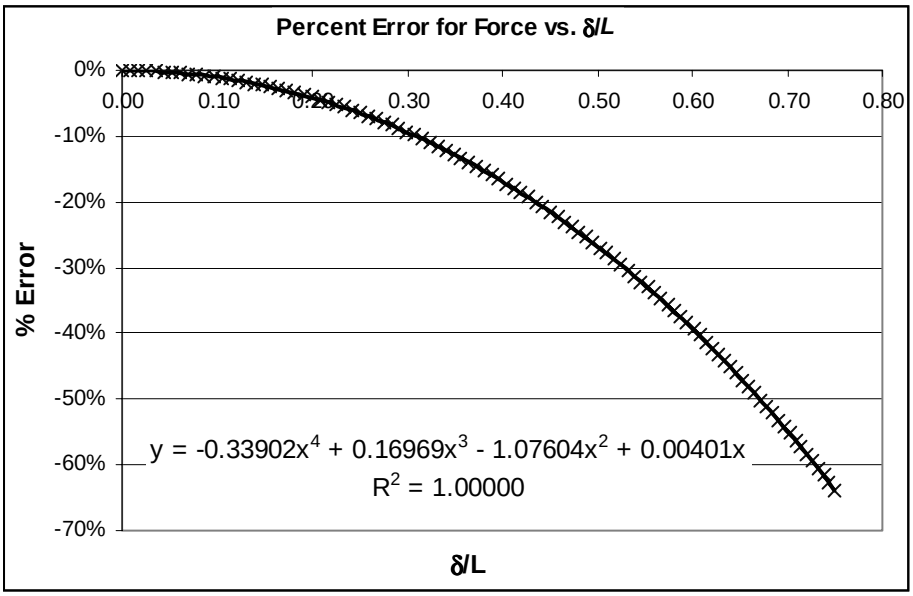

Figure 3.1 Curve fit for finding percent error for a given δ/L.

where ε_P is given by the following fitted equation:

$$\varepsilon_P = 0.00401\left(\frac{\delta}{l}\right) - 1.07604\left(\frac{\delta}{l}\right)^2 + 0.16969\left(\frac{\delta}{l}\right)^3 - 0.33902\left(\frac{\delta}{l}\right)^4 \tag{3.5}$$

The same process can be used to find a simplified explicit equation for the maximum stress in the beam (Figure 3.2). For small deflections, the maximum stress in the beam is:

$$S_{max} = \frac{Mc}{I} = \frac{6PL}{wh^2} \tag{3.6}$$

After substituting equation (3.2) in for *P*, the simplified explicit equation is

$$S_{max} = \frac{3Eh\delta}{4L^2}\frac{1}{1+\varepsilon_S} \tag{3.7}$$

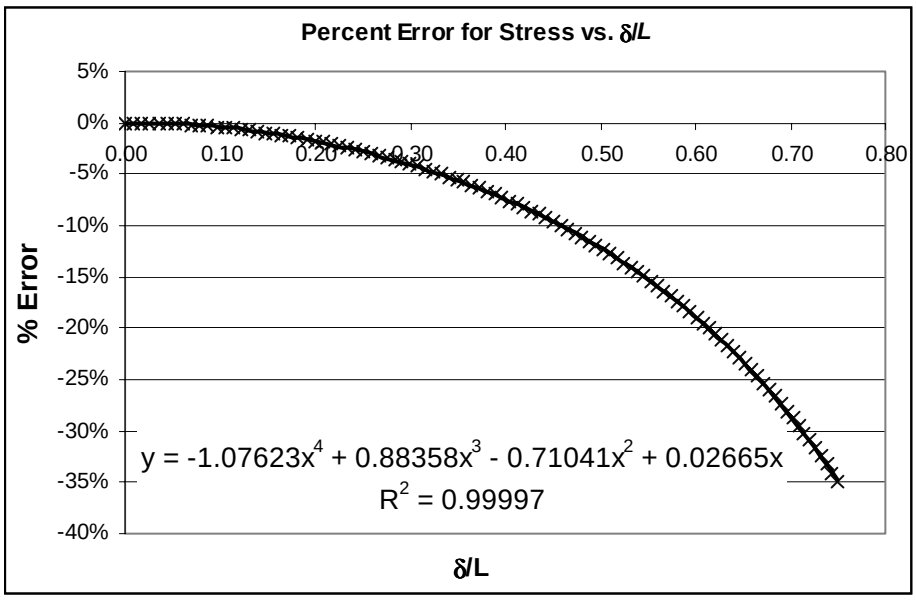

Figure 3.2 Curve fit for finding percent error in stress for a given δ/L.

where ε_S is given by the following .fitted equation:

$$\varepsilon_S = 0.02665\left(\frac{\delta}{l}\right) - 0.71041\left(\frac{\delta}{l}\right)^2 + 0.88358\left(\frac{\delta}{l}\right)^3 - 1.07623\left(\frac{\delta}{l}\right)^4 \tag{3.8}$$

The curve fits for equations (3.5) and (3.8) have R^2 values of 1.00000 and 0.99997, respectively. There is some round-off error when using the coefficients of these equations. Including this round-off error with the error inherent in the fitted curve, the accuracy of these equations can be found through a comparison to the elliptic integral solution. For $0 < \delta/L < 0.75$, the percent error for force is less than 0.03% and less than 0.32% for the maximum stress. In addition to finding the error between the linear force-deflection equations and the non-linear elliptic integral solution, equations (3.5) and (3.8) can be used to find a general rule of thumb for the limits of the uncorrected linear equations. For example, if an

error of less than 1.0% for force is desired using equation (3.2), then δ/L must be less than about 0.1. Equations (3.4) and (3.7) can be applied to any beam that is linearly elastic, isotropic, homogeneous, and has a constant rectangular cross section.

3.3 Application: Force Gauge Uncertainty Analysis

Many micro mechanisms require force measurements to determine the behavior of a system or validate theoretical predictions. Friction forces, actuator forces, and contact forces are some examples the important forces to be measured in MEMS. Fabrication of tools for measuring micro forces is complicated by the additional sources of uncertainty involved in surface micromachining processes. To obtain accurate and reliable measurements of on-chip micro forces, the uncertainty in dimensional and material parameters must be included in the error analysis.

3.3.1 General Force Gauge Model

The general force gauge shown in Figure 3.3 consists of a symmetric array of beams in parallel and/or series that acts as a spring. A displacement, d, is used to determine the applied force, F. N_p is the number of beams in parallel, and N_s is the number of sets of parallel beams in series on each side of the gauge. The mechanism or system to be tested can be connected at point B and the force applied by probe at point A. This model can describe an infinite number of possible configurations, one of which was demonstrated in Yeh and Pister (1995).

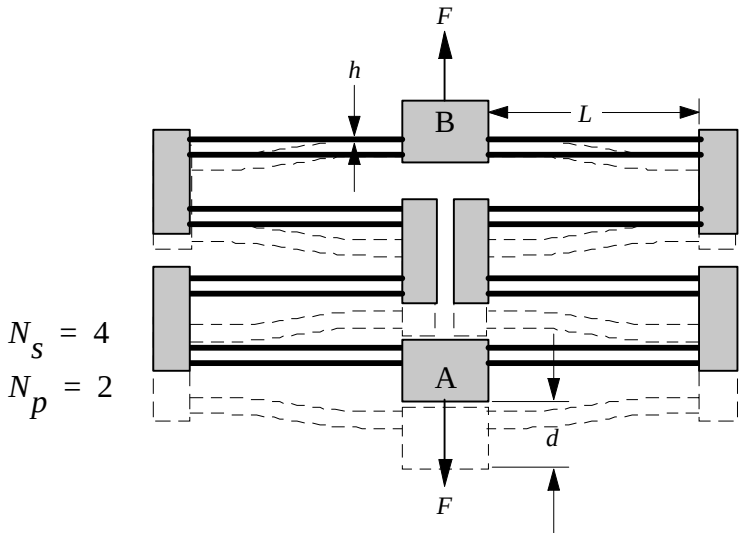

Figure 3.3 General force gauge model.

Figure 3.4 shows the free-body diagrams used to simplify the force gauge model. Each beam of the force gauge can be modeled as a fixed-guided flexible segment (or constant end angle) with $P = F/(2N_p)$, and a resultant moment, M_o. The deflected beam has an inflection point at its center where the curvature is zero. According to the Bernoulli-Euler assumption which states that the moment is directly proportional to the curvature, the moment will be zero at this inflection point. This allows the beam to be simplified to a vertically end-loaded cantilever beam with deflection $\delta = d/(2N_s)$ and length $l = L/2$ as shown in Figure 3.4.

The equations for calculating the force come from the simplification of the model to a cantilever beam with applied force, *P*, and deflection, δ, as shown in Figure 3.4c. Assuming the cross-section is rectangular and the deflection in each individual beam is

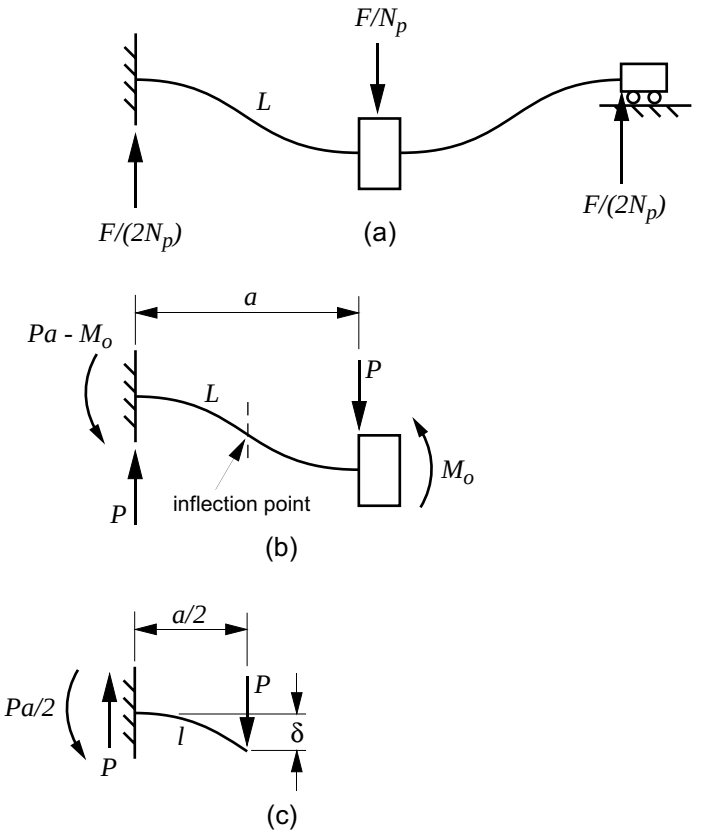

Figure 3.4 Free-body diagrams for (a) one 'leg' of the force gauge, (b) a fixed-guided flexible segment, and (c) a vertically end-loaded cantilever beam.

small, the force and maximum stress for the gauge are calculated using the following explicit equations:

$$F = \frac{N_p}{N_s}\frac{2Ewh^3d}{L^3}\frac{1}{1+\varepsilon_P} \tag{3.9}$$

$$S_{max} = \frac{3Ehd}{N_s L^2}\frac{1}{1+\varepsilon_S} \tag{3.10}$$

where the moment of inertia is $(wh^3)/12$, w is the out-of-plane thickness of the beam, h is the in-plane width of the beam, E is Young's modulus, d is the overall gauge deflection,

L is the length of the beam as shown in Figure 3.3, and ε_P and ε_S are the error functions given by equations (3.5) and (3.8).

3.3.2 Standard Deviation Values

The dimensional variations and material properties will vary with the process used to fabricate the force gauges. In this example, the force gauge was fabricated using MUMPs™. For this process, Sharpe et al. (1999) have measured a value of 162 ± 14 GPa for Young's modulus and 1.56 ± 0.25 GPa for tensile strength. Typical engineering practice is to report the plus/minus values at the 95% confidence limit, or approximately 1.96 standard deviations. Using this assumption, the standard deviations for Young's modulus and tensile strength are approximately σ_E = 7.143 GPa and σ_{Sy} = 0.128 GPa.

The tolerances for the individual layer thicknesses can be found in the MUMPs™ Design Handbook (Koester et al., 2000), discussed in Section 2.2.5. For w = 2.0 μm (Poly1), σ_w = 0.050 μm. For w = 1.5 μm (Poly2), σ_w = 0.033 μm. For w = 3.5 μm (Poly1+Poly2), σ_w = 0.060 μm.

The variation of the in-plane width of the beams is determined by a combination of the surface roughness and side-wall angle variation, as discussed in Section 2.2.5. A side-wall angle between 89 and 90 degrees combined with the surface roughness results in

approximately σ_h = 0.05 μm. Although the variation in the beam lengths is very small, a value of 0.1 μm will be used for σ_L. This results in $\sigma_l = \sigma_L/2$ = 0.05 μm.

The uncertainty in the displacement measurement will vary greatly depending upon the equipment being used. Using an optical microscope, a conservative value for the standard deviation in the displacement measurement is σ_d = 0.5 μm. This results in $\sigma_\delta = \sigma_d/(2N_s)$ = 0.25 μm.

For the example micro force gauge described in this thesis, the nominal values and standard deviations are summarized in Table 3.1.

3.3.3 Variance and Sensitivity Equations

Using the explicit force gauge equations (3.9) and (3.10) for nonlinear deflections, the variance for force and stress are calculated as follows:

$$\sigma_{F'}^2 = \left(\frac{\partial F}{\partial E}\right)^2 \sigma_E^2 + \left(\frac{\partial F}{\partial w}\right)^2 \sigma_w^2 + \left(\frac{\partial F}{\partial h}\right)^2 \sigma_h^2 + \left(\frac{\partial F}{\partial \delta}\right)^2 \sigma_\delta^2 + \left(\frac{\partial F}{\partial l}\right)^2 \sigma_l^2 \tag{3.11}$$

$$\sigma_S^2 = \left(\frac{\partial S}{\partial E}\right)^2 \sigma_E^2 + \left(\frac{\partial S}{\partial h}\right)^2 \sigma_h^2 + \left(\frac{\partial S}{\partial \delta}\right)^2 \sigma_\delta^2 + \left(\frac{\partial S}{\partial l}\right)^2 \sigma_l^2 \tag{3.12}$$

TABLE 3.1 Nominal values and standard deviations for the example micro force gauge.

	Nominal	σ	Units
L	150	0.1	μm
w	3	0.06	μm
h	3.5	0.05	μm
d	2 to 20	0.5	μm
δ	1 to 10	0.25	μm
E	162	7.143	GPa
S_y	1.56	0.128	GPa

where

$$\frac{\partial F}{\partial E} = \frac{N_p}{2}\frac{wh^3\delta}{l^3}\frac{1}{1+\varepsilon_P} \tag{3.13}$$

$$\frac{\partial F}{\partial w} = \frac{N_p}{2}\frac{Eh^3\delta}{l^3}\frac{1}{1+\varepsilon_P} \tag{3.14}$$

$$\frac{\partial F}{\partial h} = \frac{N_p}{2}\frac{3Ewh^2\delta}{l^3}\frac{1}{1+\varepsilon_P} \tag{3.15}$$

$$\frac{\partial F}{\partial \delta} = \frac{N_p}{2}\frac{Ewh^3}{l^3}\left[\frac{(1+\varepsilon_P)-\delta(\partial\varepsilon_P/\partial\delta)}{(1+\varepsilon_P)^2}\right] \tag{3.16}$$

$$\frac{\partial F}{\partial l} = -\frac{N_p}{2}\frac{Ewh^3\delta}{l^4}\left[\frac{3(1+\varepsilon_P)+l(\partial\varepsilon_P/\partial l)}{(1+\varepsilon_P)^2}\right] \tag{3.17}$$

$$\frac{\partial S}{\partial E} = \frac{3h\delta}{2l^2}\frac{1}{1+\varepsilon_S} \tag{3.18}$$

$$\frac{\partial S}{\partial h} = \frac{3E\delta}{2l^2}\frac{1}{1+\varepsilon_S} \tag{3.19}$$

$$\frac{\partial S}{\partial \delta} = \frac{3Eh}{2l^2}\left[\frac{(1+\varepsilon_S)-\delta(\partial\varepsilon_S/\partial\delta)}{(1+\varepsilon_S)^2}\right] \tag{3.20}$$

$$\frac{\partial S}{\partial l} = -\frac{3Eh\delta}{2l^3}\left[\frac{2(1+\varepsilon_S)+l(\partial\varepsilon_S/\partial l)}{(1+\varepsilon_S)^2}\right] \tag{3.21}$$

and for $i = P$ or S,

$$\frac{\partial \varepsilon_i}{\partial \delta} = \frac{C_{i1}}{l} + \frac{2C_{i2}\delta}{l^2} + \frac{3C_{i3}\delta^2}{l^3} + \frac{4C_{i4}\delta^3}{l^4} \tag{3.22}$$

$$\frac{\partial \varepsilon_i}{\partial l} = -\frac{C_{i1}\delta}{l^2} - \frac{2C_{i2}\delta^2}{l^3} - \frac{3C_{i3}\delta^3}{l^4} - \frac{4C_{i4}\delta^4}{l^5} \tag{3.23}$$

where C_{i1}, C_{i2}, C_{i3}, and C_{i4} are the coefficients of equations (3.5) and (3.8).

3.3.4 Results

Table 3.2 shows the results of the error analysis for force and stress at different deflections. $F_{elliptic}$ and $S_{elliptic}$ are the theoretically exact force and stress for the given deflection, based upon an elliptic integral solution for nonlinear deflections. This comparison was done to show how closely equations (3.9) and (3.10) approximate the nominal force and stress. The standard deviations for force and stress, σ_F and σ_S, were calculated using the method described in the previous section. The uncertainties are then represented as the *nominal value* ± *the standard deviation*, or $F \pm \sigma_F$ and $S_{max} \pm \sigma_S$. The percent error is

TABLE 3.2 Force and stress results by deflection.

	Deflection (d)			
	2 μm	10 μm	15 μm	20 μm
$F_{elliptic}$	108.88	546.82	824.98	1108.97
F	108.88	546.77	824.91	1108.93
σ_F	28.24	46.68	63.36	81.60
%Error	25.9%	8.5%	7.7%	7.4%
$S_{elliptic}$	129.61	649.24	976.20	1306.03
S_{max}	129.58	648.99	976.08	1306.35
σ_S	32.96	44.69	56.55	70.00
%Error	25.4%	6.9%	5.8%	5.4%
P[fracture]	0.000%	0.000%	0.002%	4.105%

the ratio of the standard deviation over the nominal value. The following observations can be made from Table 3.2:

- This particular gauge design is not well suited to making measurements at small deflections.
- Even though the maximum stress is below the fracture strength, there is still about a 4.1% chance of fracture at a gauge deflection of 20 μm.

A better understanding of how variation in the individual parameters affect the force is gained from a sensitivity analysis. This is done by comparing the terms on the right hand side of equations (3.11) and (3.12). The percent contribution is found by dividing each term by the total variance. Table 3.3 shows the variance components evaluated at a gauge deflection of 20 μm. It is seen that variance component associated with uncertainty in length is insignificant compared to that of the other random variables.

It is important to determine if the force error is constant or whether it changes with gauge deflection. The total force error at different gauge deflections is shown in Figure 3.5 along with the relative contributions of the variation in measured beam deflection (σ_d), in-

TABLE 3.3 Variance components for force and stress for a gauge deflection of 20 μm.

	Force		Stress	
	Value	Contribution	Value	Contribution
Var_E	2390.80	35.90%	3317.81	67.71%
Var_w	361.39	5.43%	n/a	n/a
Var_h	3074.33	46.17%	474.04	9.67%
Var_δ	827.33	12.42%	1104.84	22.55%
Var_l	5.04	0.08%	3.09	0.06%
Var_{Total}	6658.89		4899.78	

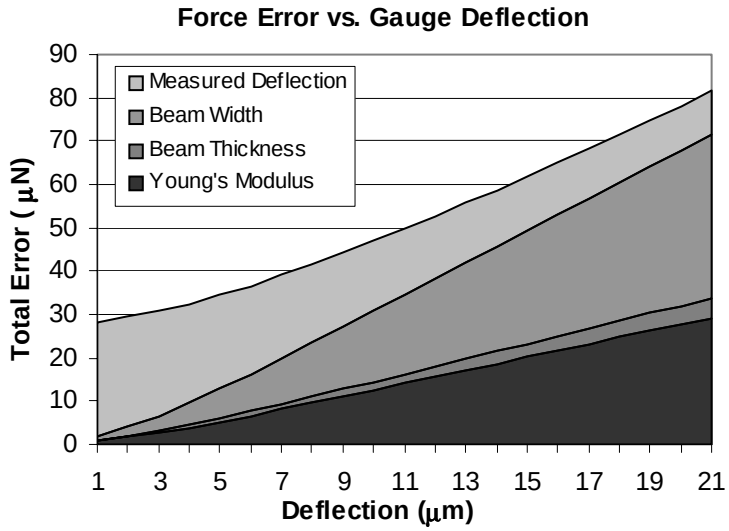

Figure 3.5 Relative contributions of the variation in δ, *h*, *w*, and *E* to the total force error at different deflections.

plane width (σ_h), beam thickness (σ_w), and Young's modulus (σ_E). The error due to variation in length was nearly zero, so it is excluded. This graph shows that the error due to σ_h, σ_w, and σ_E increases linearly with increasing deflection, while the error due to measured beam deflection increases nonlinearly.

A better way of comparing the variance components is by looking at the percent force error. It is a simple matter to show that if σ_d is taken to be zero, the percent error due to σ_l, σ_h, σ_w, and σ_E is a constant value of 6.89% in this example. However, including σ_d in the analysis affects the error significantly for small deflections. Figure 3.6 shows the percent force error vs. gauge deflection and the relative contributions of the different parameter variations. From this graph, the following observations can be made:

- For small deflections, the force error is dominated by the uncertainty in the deflection measurement.

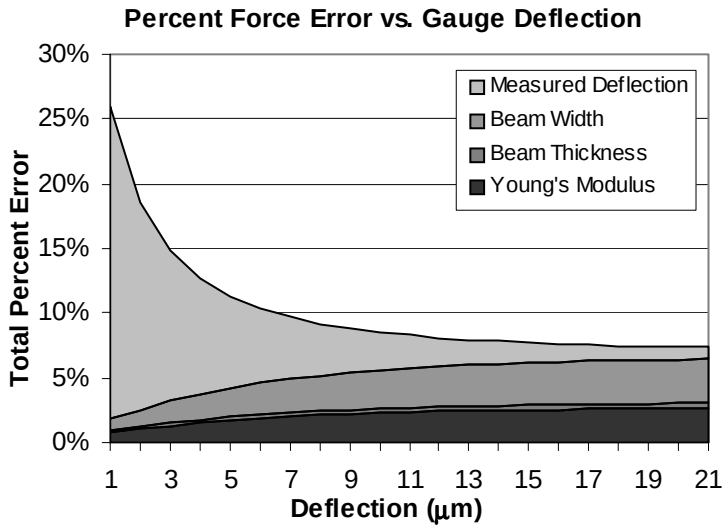

Figure 3.6 Contribution of the relative variation in δ, h, w, and E to the overall force uncertainty at different deflections.

- For large deflections, the force error is dominated by the uncertainty in in-plane width (h) and Young's modulus.

These results would suggest that the first step in improving the accuracy of the force gauge is to design it for large deflections in the range of force that is required. Any further reduction in error would require knowing Young's modulus with more certainty, reducing the beam width variation (σ_h), or performing design synthesis on the mechanism coupled with optimization to give the best combination of h, w, L, N_s, and N_p. Choosing a design to give a minimum uncertainty is therefore not trivial, but as a general rule, decreasing the ratio of σ_i to the nominal parameter value will also decrease the force uncertainty. This means that if nothing can be done to alter the uncertainty in Young's modulus, the force uncertainty can still be decreased by increasing h.

3.4 Summary

This chapter discussed the theory of uncertainty analysis and demonstrated how it is applied to explicit equations with random variables, using a vertically end-loaded cantilever beam as an example. A method for simplifying nonlinear beam deflection equations was demonstrated and applied to the explicit uncertainty analysis of a micro force gauge. It was found that uncertainty in Young's modulus and cross-section dimensions do contribute to the overall force error in the compliant micro gauge.

CHAPTER 4

THE DIRECT LINEARIZATION METHOD

The previous chapter demonstrated how to determine the statistical error in compliant members using explicit equations. Before looking at compliant mechanisms, this chapter will discuss how to determine the statistical position error in assemblies and linkages using the Direct Linearization Method (DLM). This method will be validated by comparing it to various other deterministic and probabilistic error analysis methods. A multiple loop mechanism will be used as an example.

4.1 Introduction

When analyzing the position error in kinematic linkages, the goal is usually to find error bands around an ideal path. Error bands were first developed by Garrett and Hall (1969), where they were applied to a function generating four-bar mechanism. When applied to coupler point position, there are numerous methods for determining the magnitudes of these error bands, involving both deterministic and probabilistic approaches.

An approach common to both deterministic and statistical methods is sensitivity analysis, where the sensitivity represents how the position will change with a change in an input parameter. An efficient method used in assembly tolerance analysis, called the Direct Linearization Method (DLM) (Marler, 1988; Chase et al., 1995), is based upon the linearization of a system of vector loop equations, representing an assembly, to obtain a sensitivity matrix. Kinematic joints may be inserted between mating surfaces to include the effects of small kinematic adjustments.

A common method in kinematic analysis is the use of a Jacobian matrix to analyze the sensitivity of position error with respect to individual tolerances (Cleghorn et al., 1993). These two methods are based upon the same mathematical principles, but the DLM is very general and easy to automate.

Another approach common to both deterministic and statistical methods is to solve for the position of a mechanism after making small adjustments to the component dimensions. A vertex analysis is used to determine the worst-case position error by trying all possible combinations of extreme tolerance values (Fenton et al., 1989). Monte Carlo simulation is a statistical approach where the variations are represented by probability distribution functions, with sets of parts selected randomly and assembled mathematically to obtain the predicted variation of critical assembly features.

There are several methods for estimating position error in linkages, and each method has advantages and disadvantages. For example, Monte Carlo simulations are computationally expensive, but may be applied to highly nonlinear systems. They are also

useful in validating other statistical methods (Gao et al., 1995) and determining the actual distribution of error. As a tool for use in design of kinematic linkages, a variational model for estimating position error should:

- Be general enough to apply to any 2-D or 3-D model that can be represented using vector loops.
- Be computationally efficient, so it can be implemented in kinematic analysis packages and used for design iteration.
- Be able to provide both worst-case and statistical results.

This chapter will show how the Direct Linearization Method meets these requirements.

4.2 General Linkage Model

The example used to compare the various error analysis methods is shown in Figure 4.1. Point *P* is designed to follow a specific path as the input crank (link 6) is rotated.

The nominal position of point *P* for a given input crank angle, θ_6, is found by solving two closed vector loop equations and one open vector loop equation. The two closed vector-loops are:

$$\boldsymbol{r_6} + \boldsymbol{r_7} - \boldsymbol{r_8} - \boldsymbol{r_5} = 0 \text{ and} \tag{4.1}$$

$$\boldsymbol{r_2} + \boldsymbol{r_3} - \boldsymbol{r_4} - \boldsymbol{r_1} = 0 \tag{4.2}$$

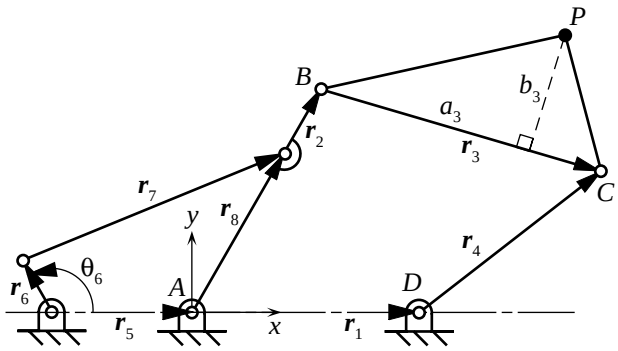

r_1 = 2.36 cm $r_2 = \overrightarrow{AB}$ = 1.33 cm r_3 = 5.08 cm r_4 = 3.94 cm

r_4 = 3.94 cm r_5 = 1.00 cm r_6 = 0.45 cm r_7 = 1.50 cm

r_8 = 1.00 cm a_3 = 6.00 cm b_3 = 0.50 cm

Figure 4.1 Double-rocker four-bar mechanism with driving crank.

where each vector $\mathbf{r}_i$ has a magnitude of r_i and an angle of θ_i measured counterclockwise from the positive *x* axis.

These equations are expanded into four equations representing the sum of the vector components in each of the two dimensions:

$$h_1 = r_6\cos\theta_6 + r_7\cos\theta_7 - r_8\cos\theta_2 - r_5 = 0 \tag{4.3}$$

$$h_2 = r_6\sin\theta_6 + r_7\sin\theta_7 - r_8\sin\theta_2 = 0 \tag{4.4}$$

$$h_3 = r_2\cos\theta_2 + r_3\cos\theta_3 - r_4\cos\theta_4 - r_1 = 0 \tag{4.5}$$

$$h_4 = r_2\sin\theta_2 + r_3\sin\theta_3 - r_4\sin\theta_4 = 0 \tag{4.6}$$

where all angles are measured counterclockwise from the positive x-axis. Equations (4.3) through (4.6) represent a nonlinear implicit set of equations with four unknown angles, θ_2, θ_3, θ_4, and θ_7. The unknown angles can be found using a nonlinear equation solver, which

is necessary in order to find the nominal position of point *P* for a given crank angle. An alternative method for this specific example is to treat the mechanism as two individual four-bar mechanisms and solve for the angles explicitly. Still another method is to use an accurate CAD layout and a query of the CAD system to obtain the nominal angles.

After equations (4.3) through (4.6) have been solved, the nominal position of point *P* is found using the following open-loop equations representing the sum of the vector components in each of the two dimensions:

$$P_x = r_2\cos\theta_2 + a_3\cos\theta_3 + b_3\cos(\theta_3 + 90°) \tag{4.7}$$

$$P_y = r_2\sin\theta_2 + a_3\sin\theta_3 + b_3\sin(\theta_3 + 90°) \tag{4.8}$$

Links one through four have an associated tolerance of ±0.03 cm and the other dimensions are treated as exact to simplify this example. The analysis of this mechanism considering tolerances on all of the dimensions can be found in Appendix A. It will be assumed that the actual dimensions are normally distributed, with a mean equal to the nominal link length and a standard deviation of 0.01 cm. This case represents a 3-sigma process, where the standard deviation is one third of the symmetric tolerance value.

Position error in linkages normally consists of both structural and mechanical error. Mechanical error occurs when the link lengths exhibit dimensional errors due to production. Structural error is present even when all the link lengths are precisely constructed. It arises from the inability of the ideal linkages to describe exactly the desired path for *P*. The structural error will not be considered in this thesis since the exact configuration of the mechanism is not the main issue. The mechanical or position error will therefore repre-

sent the deviation of point *P* from the ideal position, where the ideal position is found from the nominal values of the input parameters.

4.3 Direct Linearization Method

When applied to kinematic linkages, the Direct Linearization Method can predict position error using the implicit system of open and closed vector loops. This is done by deriving the sensitivity matrix and then applying either worst-case or statistical approaches to determine the magnitudes of position error.

4.3.1 Sensitivity Matrix

The first step is to derive the assembly equations, which for the example in this chapter are equations (4.3) through (4.6). These equations are then linearized using a first-order Taylor's series expansion. This is written as:

$$[A]\{\Delta X\} + [B]\{\Delta U\} = \{\mathbf{0}\} \tag{4.9}$$

where $\{X\}$ is the vector of independent variables $\{X\} = \{r_1, r_2, r_3, r_4\}$, $\{U\}$ is the vector of dependent variables $\{U\} = \{\theta_2, \theta_3, \theta_4, \theta_7\}$, and [*A*] and [*B*] are (4 x 4) matrices of first-order partial derivatives with respect to the independent and dependent variables, respectively:

$$[A] = (\partial h_i)/(\partial X_j) \tag{4.10}$$

$$[B] = (\partial h_i)/(\partial U_j) \tag{4.11}$$

Equation (4.9) is then solved using linear algebra to obtain the variations in the independent variables:

$$\{\Delta U\} = -[B]^{-1}[A]\{\Delta X\} \tag{4.12}$$

This same procedure is then applied to the system of open vector loops, equations (4.7) and (4.8) to obtain

$$\{\Delta P\} = [C]\{\Delta X\} + [D]\{\Delta U\} \tag{4.13}$$

where $[C]$ and $[D]$ are the first-order partial derivatives with respect to the independent and dependent variables:

$$[C] = (\partial P_i)/(\partial X_j) \tag{4.14}$$

$$[D] = (\partial P_i)/(\partial U_j) \tag{4.15}$$

where P_i is $\{P_x, P_y\}$, the coordinates of the coupler point.

Equation (4.12) is then substituted into equation (4.13) to obtain

$$\{\Delta P\} = ([C] - [D][B]^{-1}[A])\{\Delta X\} = [S_{ij}]\{\Delta X\} \tag{4.16}$$

where $[C - DB^{-1}A]$ is the variation sensitivity matrix, S_{ij}, describing how changes in the independent variables affect the position error. The expanded solution for the example in this paper is listed in Appendix A.

4.3.2 Position Error

After obtaining the sensitivity matrix, it is a relatively simple matter to determine position error using either a deterministic (worst-case) or probabilistic (statistical) approach.

The worst-case position error is found using the following equation:

$$\Delta P_i = \sum_{j=1}^{n} |S_{ij}| \text{tol}_j \tag{4.17}$$

where S_{ij} is the sensitivity matrix found from equation (4.16) and tol_j is the tolerance associated with the jth independent variable.

The statistical position error is estimated using the following equation:

$$\sigma_{P_i}^2 = \text{Var}(P_i) = \sum_{j=1}^{n} (S_{ij})^2 (\sigma_j)^2 \tag{4.18}$$

where σ_j is the standard deviation of the jth independent variable, $\text{Var}(P_i)$ is the position variance for the ith dimension. For a three-sigma estimate of position error, the standard deviation (which is the square root of the variance) is simply multiplied by three, since in this example all the tolerances represent the three-sigma manufacturing process limits.

4.3.3 Comparison to Deterministic Methods

In order to verify the DLM method for use in determining worst-case position error, it was compared to two other deterministic methods. The first was a vertex analysis,

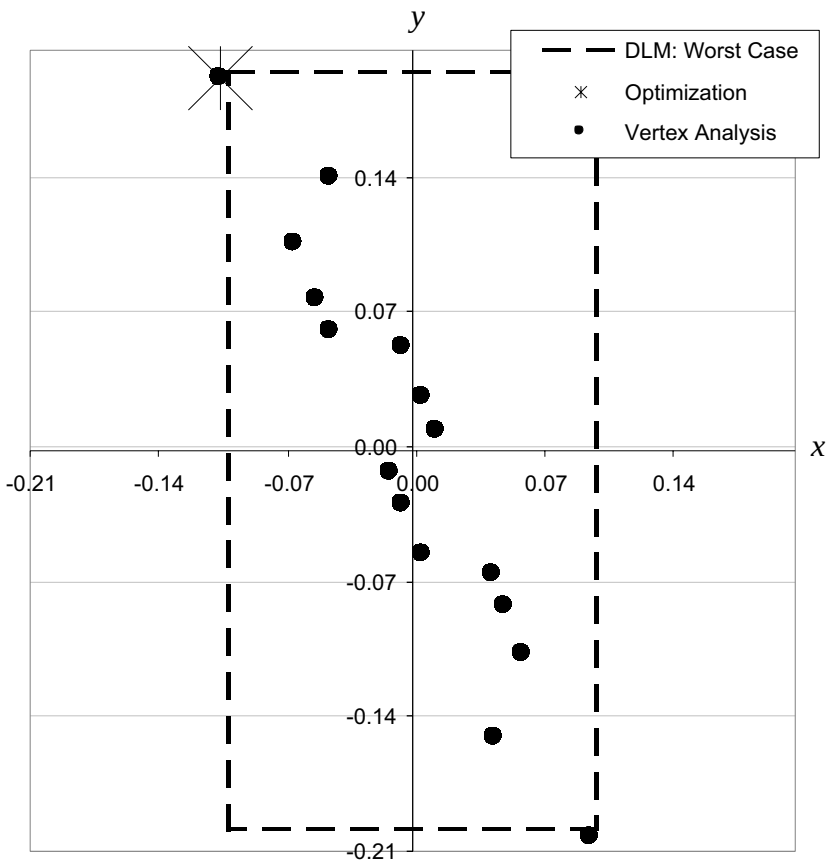

Figure 4.2 Predicted position error by deterministic methods.

where the nonlinear vector equations (4.3) through (4.8) were solved using all combinations of the extreme values of the tolerances. The second method used optimization to determine the worst possible magnitude of error given the tolerances as constraints. Both of these two methods used nonlinear solvers, whereas the DLM method uses linearization as discussed earlier. The purpose for using optimization was to determine if there were any combinations of dimension values other than extremes that could lead to worse error than predicted by the vertex analysis method.

Figure 4.2 shows the results of these three methods performed for the example mechanism at a crank position of 120 degrees. The *x* and *y* axes show the magnitude of

deviation from the expected location of the coupler point. The DLM method gives the estimated error as an error band about the nominal position, which results in a rectangle. The vertex analysis shows that almost all the points lie within this box. It is assumed that the points that lie outside of the DLM zone is a result of linearization. A very important validation of the DLM method is that the results of the optimization routine corresponds with one of the extreme values found using the vertex analysis method. At this time there is no known means of proving that this will be true for all kinematic linkages, but in every case tried so far, no exceptions have been found. Another important result of this comparison is that the vertex points are not uniformly distributed about the nominal position. The zone that circumscribes these points appears to be narrowly clustered about a sloped line of about 45 degrees. This would suggest that there is some correlation between the *x* and *y* error.

4.4 Bivariate Normal Model of Position Error Using DLM

There is a difference between the position error of a part feature and an assembly feature. For example, a hole may be located on a feature with respect to two datums, where the position error with respect to these datums are independent. However, in assemblies or kinematic linkages, the position error is generally not independent with respect to the different axes, meaning you cannot have an error in the *x* direction without introducing error in the *y* direction. An accurate model must account for this correlation.

Schade (1983) presented a bivariate normal model of mechanism coupler-point position error, where the contour of equal probability is described as an ellipse. The results

were verified using a Monte Carlo simulation. Independent research led Brown (1995) to develop a similar method for describing the position error in mechanical assemblies and these results were also verified using a Monte Carlo simulation. The main difference is that Brown developed a general model based upon DLM, while Schade provided a specific example for the case of a four-bar mechanism. A detailed comparison of the two methods found them to be in agreement, adding validity to use of DLM for general use in kinematic position error analysis.

4.4.1 Contours of Equal Probability

The essential ingredient to extend the DLM method to a bivariate normal model is the use of covariance. The two-dimensional position error at a given point on a coupler path can be described using a symmetric variance matrix:

$$\begin{bmatrix} V_x & V_{xy} \\ V_{xy} & V_y \end{bmatrix} \tag{4.19}$$

where V_x and V_y are found using equation (4.18) and V_{xy} is found using the following equation:

$$V_{xy} = \sum_{j=1}^{n} (S_{ij})(S_{ji})\sigma_j^2 \tag{4.20}$$

The variance matrix is important because its eigenvalues indicate the magnitude and direction of greatest variation. The eigenvalues are principle variances that represent

the major and minor diameters of an elliptic contour of equal probability (Schade 1983). Solving the eigenvalue problem leads to the principle variances:

$$V_1 = \frac{V_x + V_y}{2} + \sqrt{V_{xy}^2 + \left(\frac{V_y - V_x}{2}\right)^2} \tag{4.21}$$

$$V_2 = \frac{V_x + V_y}{2} - \sqrt{V_{xy}^2 + \left(\frac{V_y - V_x}{2}\right)^2} \tag{4.22}$$

with $2\sigma_1 = 2\sqrt{V_1}$ being the major ellipse diameter and $2\sigma_2 = 2\sqrt{V_2}$ being the minor ellipse diameter. The angle of rotation of the y-axis to a principle axis is found using:

$$\theta_R = \frac{1}{2}\tan^{-1}\left(\frac{2V_{xy}}{V_y - V_x}\right) \tag{4.23}$$

Using the inverse tangent function, which gives an angle from -90 to 90 degrees, only finds the rotation of the y-axis to one of the principle axis, without a distinction of whether the axis is the major or minor ellipse diameter. This problem can be solved using an "arctan2" function that determines the angle from -180 to 180.

When V_{xy} is zero, the principle axes correspond to the *x* and *y* coordinate axes. In this case, the equation of the ellipse is simply

$$\frac{\Delta x^2}{\sigma_2^2} + \frac{\Delta y^2}{\sigma_1^2} = n^2 \tag{4.24}$$

where n is the sigma-level of the process. Each value of n gives a different contour of equal probability. Converting this equation to polar coordinates allows for a simple method of accounting for a nonzero V_{xy}:

$$\frac{\cos^2(\theta - \theta_R)}{\sigma_2^{\,2}} + \frac{\sin^2(\theta - \theta_R)}{\sigma_1^{\,2}} = \frac{n^2}{r^2} \tag{4.25}$$

where $\Delta x = r\cos(\theta - \theta_R)$ and $\Delta y = r\sin(\theta - \theta_R)$, and θ_R is the rotation angle found using equation (4.23). If $\sigma_1 = \sigma_2$, then equation (4.25) becomes the equation of a circle with radius n/r. In this case, the magnitude of variance is constant in all directions, and the error bands are simple to determine. However, for elliptic contours, the magnitude of variance may vary widely with direction. In these cases, it is common to create error bands that represent the maximum normal distance to the coupler path, since variation parallel to the path is of no consequence, (unless points on the path must be indexed to positions of the input crank).

This is done by solving for the points on the ellipse whose tangents have the same slope as the coupler path. It is not difficult to solve for the point on the ellipse that is the maximum normal distance from the path slope, if the principle axes of the ellipse are used as a reference coordinate system. The slope of the tangent at any point on the ellipse can be found from equation (4.24) as:

$$\text{slope} = -\frac{1}{\tan(\theta)}\frac{V_1}{V_2} \tag{4.26}$$

If the slope of the coupler path in the reference frame of the ellipse is $m_o = \tan(\theta_m - \theta_R)$, then the angle $(\theta - \theta_R)$ that represents the point on the ellipse at the maximum normal distance from the coupler path is:

$$(\theta - \theta_R) = \tan^{-1}\left(-\frac{1}{m_o}\frac{V_1}{V_2}\right) \tag{4.27}$$

Equation (4.25) is then used to solve for *r*, Δx, and Δy and the results are then transformed to the original coordinate frame.

Finding the yield, or the probability that the position will be within a contour of equal probability, is simple for the bivariate normal distribution. The bivariate normal model for two-dimensional position error uses the chi-squared distribution, $\chi^2(n^2, \nu)$, with $\nu = 2$ degrees of freedom, evaluated at *n*, where *n* is the sigma level. Whereas a 3-sigma one-dimensional normal distribution yields 99.73%, a 3-sigma bivariate normal distribution yields 98.89%.

4.4.2 Comparison to Monte Carlo

In order to verify the DLM method for use in statistical position error, it was compared to a Monte Carlo simulation. Both the root-sum-square (RSS) DLM approach and the bivariate normal model were used and Figure 4.3 shows the results of these three methods performed for the example mechanism at a crank position of 120 degrees. A sigma level of 3 was used in the example. A more detailed comparison of the RSS approach with Monte Carlo was also done in an earlier study by Gao et al. (1995) for a variety of assemblies. The results of this study showed that if the tolerances are small rela-

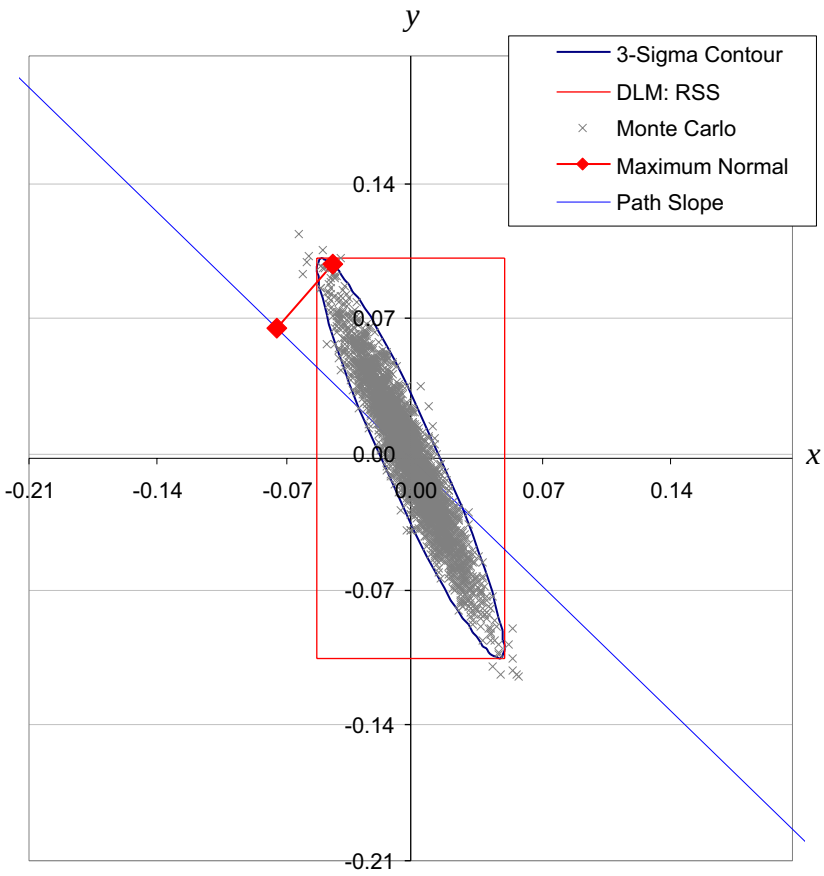

Figure 4.3 Comparison of statistical methods.

tive to the nominal dimensions, and if the assembly equations are not highly nonlinear, then DLM is accurate.

Brown (1995) extended the DLM to find ΔP_x and ΔP_y for position variation, and applied equation (4.18) to obtain V_{xy} from the DLM sensitivity matrix. He concluded that the position variation contour was an ellipse, not a rectangle. If you simply apply ΔP_x and ΔP_y without calculating the covariance, you get a box, which predicts the limits with reasonable accuracy, but cannot predict the yield or percent rejects.

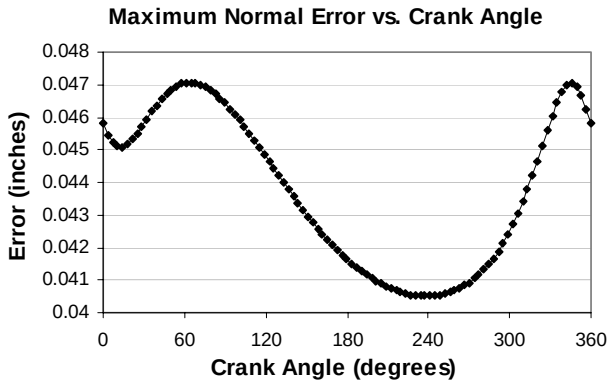

Figure 4.4 Maximum normal (perpendicular) position error evaluated over a complete crank cycle.

The Monte Carlo simulation, which used 100,000 data points, resulted in 98.876% being within the 3-sigma bivariate ellipse. The shading in Figure 4.3 is due to the density of points falling within the ellipse. The expected result was 98.889% based on the χ^2 distribution. This is actually a very good result considering that the Monte Carlo simulation was based upon the nonlinear solution, whereas the bivariate model used direct linearization. This validation is important because DLM is much more efficient than Monte Carlo simulations, and can be automated for use in computer software (Chase et al., 1995). For mechanisms, where the position error is determined at multiple points over the range of motion, it is essential that an efficient method be used. Figure 4.4 shows the 3-sigma maximum normal (perpendicular) position error evaluated at 100 crank positions using the direct linearization method as discussed in section 4.1. The same analysis using Monte Carlo Simulation would have taken at least 5000 times as long.

4.4.3 Statistical vs. Deterministic Methods

Figure 4.5 compares the bivariate normal model to the deterministic models discussed earlier, with three contours of equal probability: $n = 3$, $n = 4.5$, and $n = 6$ sigma. The corresponding yield for these contours based upon the χ^2 distribution would be 98.889%, 99.996%, and 99.999998%. These results suggest that the 6-sigma bivariate model could be an alternative approach to using the deterministic methods for worst-case error analysis. Not only is it conservative, but it gives a better representation of the actual error zone and can be used to solve for the maximum perpendicular variation.

An interesting result of comparing statistical to deterministic methods is that when using direct linearization, the error introduced due to linearization is almost insignificant. This is because the stack-up of tolerances reduces the probability of reaching the absolute worst case. For example, for this mechanism evaluated at the given angle, the probability of obtaining the absolute maximum found through optimization is about 1.1 in a trillion corresponding to a sigma level of 7.42. Therefore, although there is some error in the DLM worst-case method introduced through linearizing a set of nonlinear implicit equations, the significance of this error is statistically (and practically) zero.

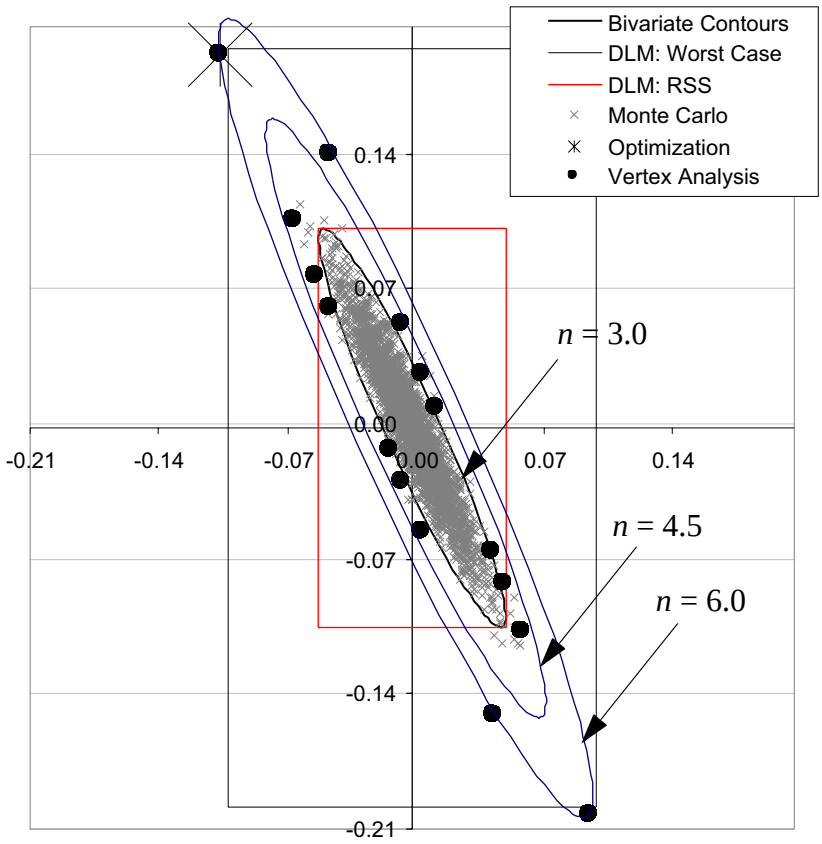

Figure 4.5 Comparison of both deterministic and probabilistic method.

4.5 Summary

The direct linearization method has been shown to be a valuable method for use in kinematic error analysis. The method of obtaining the sensitivity matrix is very general and can be used for almost any set of nonlinear implicit equations. The sensitivities can then be used to estimate the worst-case, RSS, or bivariate normal error. There will be some error introduced through linearization, especially for large tolerances, large kinematic adjustments, and highly nonlinear equations, but this error is often statistically insignificant. The main difficulty in using this method is that finding the nominal position of the

mechanism requires the nonlinear solution of the set of equations. However, when integrated with a kinematics software package, these dimensions and positions can be read directly from the computer model.

When compared to Monte Carlo simulations, vertex analysis, and optimization, the bivariate normal model has been shown to be the most efficient method of accurately representing the position error. Although this chapter focused on a two-dimensional multi-loop mechanism with one objective (position of one point), the DLM can be expanded to include multiple dimensions, multiple loops, and multiple objectives, all solved simultaneously using the same sensitivity matrix. The ease with which the sensitivity matrix is obtained for each nominal position makes it practical for use in determining the error bands for the full motion of a kinematic linkage.

CHAPTER 5

EXAMPLE OF DLM IN COMPLIANT MECHANISMS

The chapter will apply the direct linearization method (DLM) to the sensitivity analysis of compliant mechanisms. By using the pseudo-rigid-body model and force-equilibrium equations, the sensitivity of position and force error with respect to various design parameters can be determined. A partially compliant parallel mechanism will be used as an example.

5.1 Introduction

The direct linearization method is typically used to determine the effects of tolerances on assemblability or position error. However, it can be extended quite readily to include the effects of variations in cross-sectional and material parameters on the reaction forces in compliant mechanisms. As the previous chapter already explained how the sensitivity matrix is used to determine worst-case or statistical variation, this chapter will only focus on obtaining this matrix for mechanisms involving internal and external forces. The complete set of nonlinear implicit equations will consist of three sets of equations:

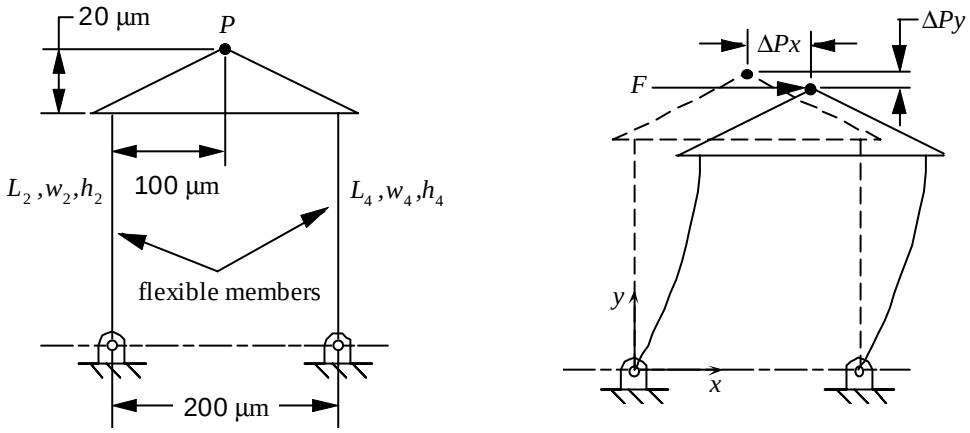

Figure 5.1 Partially compliant parallel mechanism in its (a) initial and (b) deformed positions.

1. Kinematic equations that describe the position of the mechanism
2. Static force-equilibrium equations
3. Pseudo-rigid-body model relationships

In order to validate this approach for obtaining the sensitivity matrix, the results will be compared to finite element analysis. A partially compliant parallel four-bar mechanism will be used as an example.

5.2 Partially-Compliant Parallel Mechanism

Figure 5.1 shows a partially-compliant parallel mechanism in its initial and deformed positions. The flexible members have lengths L_2 = 200 μm and L_4 = 200 μm with cross-sectional dimensions of h_2 = 3 μm, w_2 = 2 μm and h_4 = 3 μm, w_4 = 2 μm, respectively. Figure 5.2 shows the pseudo-rigid-body model with the corresponding vector

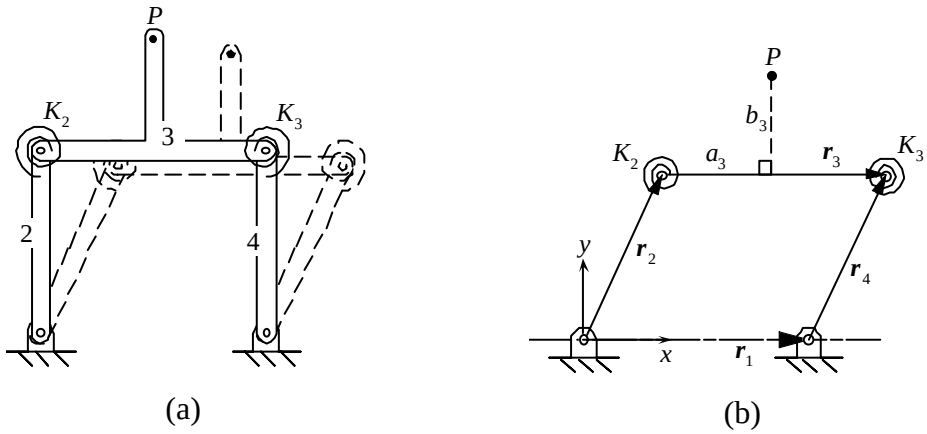

Figure 5.2 (a) Pseudo-rigid-body model and (b) the corresponding vector model.

model. Using a value of 0.85 for the characteristic radius factor, γ, gives a value of $\gamma L = 170$ μm for r_2 and r_4. To account for this change, the location of point P with respect to link 3 is $(a_3, b_3) = (100, 50)$ μm. The torsional spring constants are related to the flexible member dimensions using the following relationship for a fixed-pinned segment:

$$K = \gamma K_\Theta E \frac{wh^3}{12L} \tag{5.1}$$

Where $K_\Theta = 2.61$ and Young's modulus is E = 162000 MPa.

5.3 Constructing the Sensitivity Matrix using DLM

5.3.1 Kinematic Equations

The kinematic equations that describe the position of the pseudo-rigid mechanism consist of two equations representing the sum of the vector components in the *x* and *y* directions:

$$h_x = r_2\cos\theta_2 + r_3\cos\theta_3 - r_4\cos\theta_4 - r_1\cos\theta_1 = 0 \tag{5.2}$$

$$h_y = r_2\sin\theta_2 + r_3\sin\theta_3 - r_4\sin\theta_4 - r_1\sin\theta_1 = 0 \tag{5.3}$$

The position of the coupler point is then found from the following two equations:

$$P_x = r_2\cos\theta_2 + a_3\cos\theta_3 + b_3\cos(\theta_3 + 90°) \tag{5.4}$$

$$P_y = r_2\sin\theta_2 + a_3\sin\theta_3 + b_3\sin(\theta_3 + 90°) \tag{5.5}$$

5.3.2 Static Force-Equilibrium Equations

The pseudo-rigid-body model allows the static force-equilibrium equations to be constructed using the free-body-diagram approach. Using the generalized four-bar model

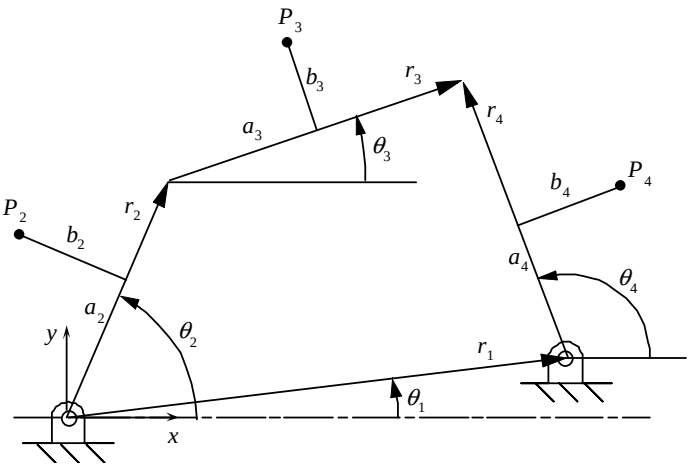

Figure 5.3 General four-bar vector model.

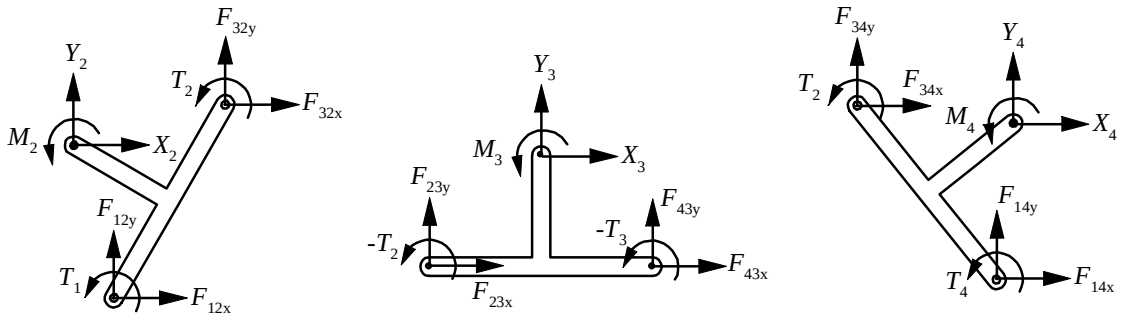

Figure 5.4 Free-body-diagrams for (a) link 2, (b) link 3, and (c) link 4.

shown in Figure 5.3, the links are separated and the equations of static equilibrium are found for each individual link (Figure 5.4).

The equations for link 2 are:

$$\sum F_x = F_{12x} + F_{32x} + X_2 = 0 \tag{5.6}$$

$$\sum F_y = F_{12y} + F_{32y} + Y_2 = 0 \tag{5.7}$$

$$\sum M_{O_1} = T_1 + T_2 + M_2 + F_{32y} r_2 \cos\theta_2 - F_{32x} r_2 \sin\theta_2 + Y_2(a_2 \cos\theta_2 + b_2 \cos(\theta_2 + 90)) - X_2(a_2 \sin\theta_2 + b_2 \sin(\theta_2 + 90)) = 0 \tag{5.8}$$

The equations for link 3 are:

$$\sum F_x = F_{23x} + F_{43x} + X_3 = 0 \tag{5.9}$$

$$\sum F_y = F_{23y} + F_{43y} + Y_3 = 0 \tag{5.10}$$

$$\sum M_A = -T_2 - T_3 + M_3 + F_{43y} r_3 \cos\theta_3 - F_{43x} r_3 \sin\theta_3 + Y_3(a_3 \cos\theta_3 + b_3 \cos(\theta_3 + 90)) - X_3(a_3 \sin\theta_3 + b_3 \sin(\theta_3 + 90)) = 0 \tag{5.11}$$

The equations for link 4 are:

$$\sum F_x = F_{14x} + F_{34x} + X_4 = 0 \tag{5.12}$$

$$\sum F_y = F_{14y} + F_{34y} + Y_4 = 0 \tag{5.13}$$

$$\sum M_{O_2} = T_3 + T_4 + M_4 + F_{34y} r_4 \cos\theta_4 - F_{34x} r_4 \sin\theta_4 + Y_4(a_4 \cos\theta_4 + b_4 \cos(\theta_4 - 90)) - X_4(a_4 \sin\theta_4 + b_4 \sin(\theta_4 - 90)) = 0 \tag{5.14}$$

Including the reaction force relationships $F_{ij} = -F_{ji}$, there are a total of 13 equations, but using substitution can reduce this set to 9 equations:

$$f_1 = F_{12x} - F_{23x} + X_2 = 0 \tag{5.15}$$

$$f_2 = F_{12y} - F_{23y} + Y_2 = 0 \tag{5.16}$$

$$f_3 = F_{23x} - F_{34x} + X_3 = 0 \tag{5.17}$$

$$f_4 = F_{23y} - F_{34y} + Y_3 = 0 \tag{5.18}$$

$$f_5 = F_{14x} + F_{34x} + X_4 = 0 \tag{5.19}$$

$$f_6 = F_{14y} + F_{34y} + Y_4 = 0 \tag{5.20}$$

$$f_7 = T_1 + T_2 + M_2 - F_{23y} r_2 \cos\theta_2 + F_{23x} r_2 \sin\theta_2 + Y_2(a_2 \cos\theta_2 + b_2 \cos(\theta_2 + 90)) - X_2(a_2 \sin\theta_2 + b_2 \sin(\theta_2 + 90)) = 0 \tag{5.21}$$

$$f_8 = -T_2 - T_3 + M_3 - F_{34y} r_3 \cos\theta_3 + F_{34x} r_3 \sin\theta_3 + Y_3(a_3 \cos\theta_3 + b_3 \cos(\theta_3 + 90)) - X_3(a_3 \sin\theta_3 + b_3 \sin(\theta_3 + 90)) = 0 \tag{5.22}$$

$$f_9 = T_3 + T_4 + M_4 + F_{34y} r_4 \cos\theta_4 - F_{34x} r_4 \sin\theta_4 + Y_4(a_4 \cos\theta_4 + b_4 \cos(\theta_4 - 90)) - X_4(a_4 \sin\theta_4 + b_4 \sin(\theta_4 - 90)) = 0 \tag{5.23}$$

Using this set of equations, there are 21 force or moment variables: 8 reaction forces (F_{ij}), 6 external forces (X_i,Y_i), 3 external moments (M_i), and 4 torques due to tor-

sional springs (T_i). Using 9 equations, only 9 unknowns can be solved for. Since the reaction forces are generally unknown, this set of equations can be used to find one unknown external force or moment if the rest of the external forces, moments, and torques are known. The benefit of using this generalized set of equations is that the partial derivatives can also be determined without having to re-derive the equations for different loading conditions.

5.3.3 Pseudo-Rigid-Body Model Relations

The final set of equations to derive before constructing the overall sensitivity matrix are those equations that relate the link lengths in the pseudo-rigid-body model (r_i) to the compliant model (L_i), and those equations that define the torsion in the springs (T_i). For the example problem, this requires four equations:

$$c_1 = -r_2 + \gamma L_2 = 0 \tag{5.24}$$

$$c_2 = -r_4 + \gamma L_4 = 0 \tag{5.25}$$

$$c_3 = T_2 + \gamma K_\Theta E \frac{w_2 h_2^{\,3}}{12 L_2}[(\theta_2 - \theta_{2o}) - (\theta_3 - \theta_{3o})] = 0 \tag{5.26}$$

$$c_4 = T_3 + \gamma K_\Theta E \frac{w_4 h_4^{\,3}}{12 L_4}[(\theta_4 - \theta_{4o}) - (\theta_3 - \theta_{3o})] = 0 \tag{5.27}$$

5.3.4 Constructing the Sensitivity Matrix

The nonlinear implicit set of equations used to find the sensitivity matrix consists of the kinematic equations (5.2) through (5.3), the static equilibrium equations (5.15)

through (5.23), and the pseudo-rigid-body model relations (5.24) through (5.27). For an applied displacement on the coupler point in the *x* direction, the vector of unknown variables is:

$$\{U\} = \{\theta_3, \theta_4, X_3, F_{12x}, F_{12y}, F_{23x}, F_{23y}, F_{14x}, F_{14y}, F_{34x}, F_{34y}, r_2, r_4, T_2, T_4\} \quad (5.28)$$

Following the steps of the DLM method, the sensitivity of any of the unknown variables with respect to a known variable can be determined by constructing the $[-B^{-1}A]$ matrix. For the sensitivity of the position of point *P* with respect to the primary variables, the $[C\text{-}EB^{-1}A]$ matrix is constructed. For this example, the vector of primary variables is:

$$\{X\} = \{r_1, L_2, r_3, L_4, a_3, b_3, w_2, h_2, w_4, h_4, E, \gamma, K_\Theta\} \quad (5.29)$$

5.3.5 Results

For a displacement of ΔP_x = 10 μm, and values for σ_i shown in Table 3.1 for the micro force gauge example, Table 5.1 shows the sensitivity and variance of the reaction force and coupler point position with respect to the above primary variables. This analysis shows that using the pseudo-rigid-body model, the position variation is extremely sensitive to the characteristic radius factor, γ (a few orders of magnitude larger than any of the

TABLE 5.1 Sensitivities and variances for force and position determined by DLM.

Force, F_x	r_1	L_2	r_3	L_4	a_3	b_3	w_2	h_2	w_4	h_4	E	γ	K_Θ
Sensitivity:	-0.217	-0.422	0.217	0.365	0.000	0.000	1.402	2.805	1.402	2.805	3.5E-05	0.000	2.149
% Variance:	7.4%	1.4%	0.4%	1.0%	0.0%	0.0%	5.5%	15.4%	5.5%	15.4%	47.9%		

Position, P_y	r_1	L_2	r_3	L_4	a_3	b_3	w_2	h_2	w_4	h_4	E	γ	K_Θ
Sensitivity:	0.029	0.423	-0.029	0.426	0.000	1.000	0.000	0.000	0.000	0.000	0.000	199.654	0.000
% Variance:	1.3%	13.0%	0.1%	13.2%	0.0%	72.6%	0.0%	0.0%	0.0%	0.0%	0.0%		

other sensitivities). In addition, the sensitivity of the force with respect to the stiffness coefficient, K_Θ, is on the same order of magnitude as a few of the other sensitivities. For this example, γ and K_Θ are assumed to be exact, so they contribute no variance to force or position. However, these parameters are not always constant, resulting in structural error in the model.

As expected, the force is sensitive to variation in the cross-sectional dimensions of the flexible beams. What is not intuitive is that the force appears to be twice as sensitive to changes in height than changes in width. The torsional spring constants involve a cubed height term and a linear width term, so the linear relationship between the sensitivities is not expected.

The sensitivities are independent of the actual amount of variation (σ_i), therefore, it is very important to consider scaling and units. For example, the sensitivity of force with respect to Young's modulus is 3.46E-05. In this example, the units for Young's modulus are MPa and the units for force are μN, so this sensitivity indicates that for an increase in *E* of 1 MPa, the force will increase by 3.46E-5 μN. However, the variation in *E* for poly-silicon is around 2000 MPa. The presents a scaling problem when comparing the different sensitivities. For this reason, a common means of comparing sensitivities is by using per-cent variance contributions. These are shown in Table 5.1 along with the sensitivities. The important point to remember here is that just because a sensitivity is small does not mean the overall contribution of the variation will also be small.

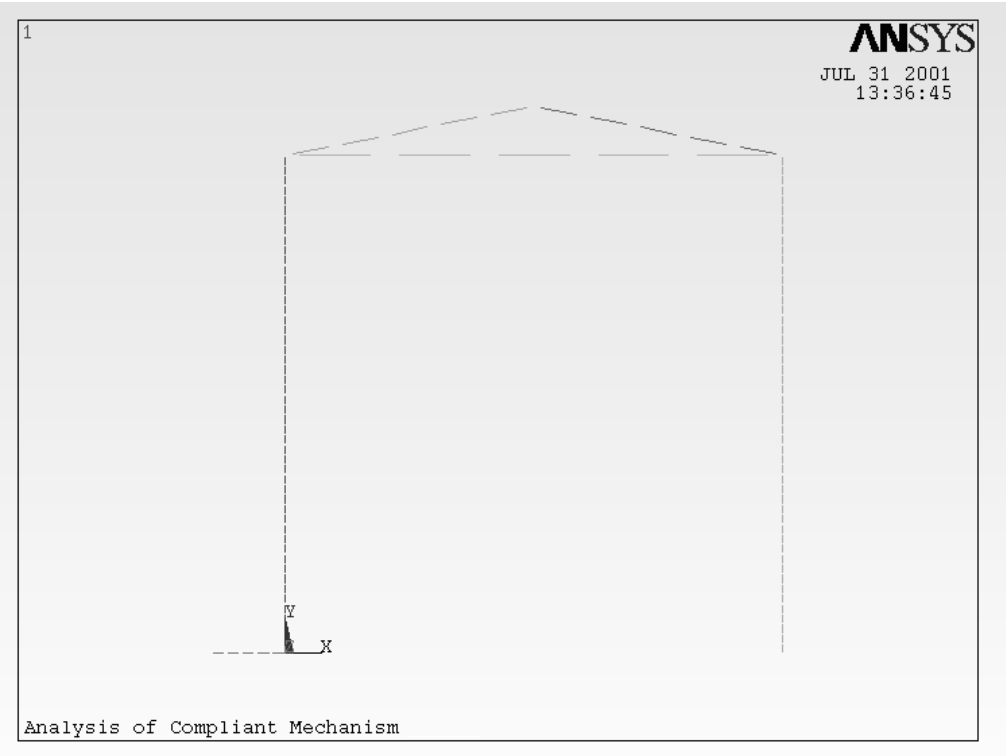

Figure 5.5 Finite element model of the example parallel mechanism.

5.4 Comparison to FEA

In order to validate the direct linearization method using the pseudo-rigid-body model, the sensitivities were compared to those found through finite element analysis.

5.4.1 The FEA model

Appendix B includes the batch file used to run an ANSYS® finite element analysis of the parallel mechanism. Figure 5.5 shows an example of the model where all the parameters are set to their nominal values and the beams are divided into elements. The flexible segments (links 2 and 4) were divided into 50 nonlinear beam elements. The sensitivities

were found using a central difference derivative approach. For example, to determine the sensitivity of the reaction force with respect to variation in link two, a separate finite element analysis is performed after adjusting the link length in the positive and negative directions. The sensitivity is found using:

$$\frac{\partial F}{\partial L_2} \approx \frac{F(L_2 + \Delta L_2) - F(L_2 - \Delta L_2)}{2\Delta L_2} \tag{5.30}$$

The variation used for each parameter was chosen to be either 0.1 μm or 2000 MPa. The analysis was run again using much smaller variations (0.001 μm and 1 MPa) to verify that the derivatives were accurate even though the problem involved nonlinearities.

Setting up the finite element model is not trivial. Care must be taken to ensure that if only one parameter is perturbed, the other parameters are not. This is important, because varying a link length will change the assembled configuration of the mechanism. There will be some initial stress and displacement caused by the link length variations, if the positions of the ground pins are held constant. To properly model this in ANSYS®, an additional load step was used to represent the assembly of the mechanism. First, the mechanism was modeled using the grounded pin of link 2 as the origin. The first load step was then to displace the other pin to the proper ground position. The resulting configuration represented the assembled state of the mechanism. Additional load steps were then used to find the reaction force at the coupler point, given various displacements in the *x* direction. These additional load steps also were required to update the stiffness matrix so as to converge to the correct solution.

5.4.2 Comparison of DLM and FEA results

For a displacement of ΔP_x = 10 μm, Table 5.2 shows the sensitivity of the reaction force and coupler point position and rotation. Considering that the pseudo-rigid-body model is only an approximation, and the system of equations was linearized using DLM, the sensitivities are very close to those found through FEA. These results suggest that just as the pseudo-rigid-body model is a good initial approximation of forces and position of a compliant mechanisms, it can also be used to determine approximate sensitivities through the use of DLM.

5.5 Summary

This chapter demonstrated how to use the direct linearization method to determine the sensitivities of a compliant mechanism with respect to geometric dimensions and material properties. In order to further validate this approach, more configurations and loading conditions ought to be investigated. The results of this research found that using

TABLE 5.2 Comparison of sensitivities found through DLM and FEA.

	F_x Sensitivity		P_Y Sensitivity		θ_3 Sensitivity	
	DLM	*FEA*	*DLM*	*FEA*	*DLM*	*FEA*
r_1	-0.22	-0.20	0.03	0.03	0.02	0.02
L_2	-0.42	-0.65	0.42	0.52	-0.24	-0.29
r_3	0.22	0.20	-0.03	-0.03	-0.02	-0.02
L_4	0.37	0.56	0.43	0.48	0.24	0.29
a_3	0.00	0.00	0.00	0.00	0.00	0.00
b_3	0.00	0.00	1.00	1.00	0.00	0.00
w_2	1.40	1.37	0.00	0.00	0.00	0.00
h_2	2.80	2.74	0.00	0.00	0.00	0.00
w_4	1.40	1.37	0.00	0.00	0.00	0.00
h_4	2.80	2.74	0.00	0.00	0.00	0.00
E	3.46E-05	3.38E-05	0.00	0.00	0.00	0.00

the pseudo-rigid-body model to construct the set of nonlinear implicit equations was feasible. However, the position variation is highly sensitive to the characteristic radius factor, γ. This implies that in order to obtain accurate results, the value of gamma must be known precisely. For some compliant mechanisms, an average or estimated value of gamma is often used. It is these cases that ought to be investigated to determine the validity of using the direct linearization method to obtain sensitivities.

This thesis has focused on the use of sensitivities to obtain the position error in mechanisms. However, these sensitivities are very important for many other applications. For example, the sensitivities can be used in optimization routines to find more robust or lower cost designs.

CHAPTER 6

CONTRIBUTIONS AND RECOMMENDATIONS

6.1 Contributions

Previous to the research presented in this thesis, very little had been done to model the effects of tolerances and clearances in micro-electro-mechanical systems (MEMS) and compliant mechanisms in general. The main contribution of this thesis was the demonstration of the plausibility of using direct linearization for determining these effects. The specific contributions of this thesis are listed below:

- Characterization of the types of variation common in micro-mechanisms.
- Method for simplifying large-deflection equations for determining mechanical error in flexible beams.
- Design of micro force gauges including an estimate of the expected resolution based upon uncertainty analysis.
- Comparison of deterministic and probabilistic methods for analyzing the position error in kinematic linkages.

- Demonstration of the use of the direct linearization method for estimating the mechanical error in kinematic linkages.
- Extension of the direct linearization method to include force-equilibrium equations and pseudo-rigid-body relationships.
- Demonstration of the plausibility of using direct linearization in the sensitivity analysis of compliant mechanisms through a comparison of the pseudo-rigid-body model and finite element analysis.

6.2 Conclusions

The main purpose of this thesis was to develop a method for determining the effects of tolerances on the mechanical error in compliant mechanisms. This thesis demonstrated that this is possible using the pseudo-rigid-body model for compliant mechanisms and applying the direct linearization method to obtain sensitivities. The use of these sensitivities in determining both worst-case and statistical results was validated by comparison with other deterministic and probabilistic methods. One of the main benefits of the direct linearization approach coupled with the pseudo-rigid-body model is the computational efficiency of the method and its potential of automation. Also, in applications such as micro mechanisms, where it is difficult to obtain accurate material properties and dimensional variations, the error analysis methods discussed in this thesis can be a great aid in designing more robust mechanical systems.

6.3 Recommendations for Further Research

The analysis methods discussed in this thesis were limited in order to provide a firm basis for further research in the sensitivity analysis of compliant mechanisms. However, this research has led to many other interesting research possibilities, some of which are listed below:

1. Application of DLM to three-dimensional kinematic linkages.

2. Use of DLM in combination with mechanism synthesis.

3. Extension of these methods to include dynamic responses.

4. Use of sensitivity analysis as a tool for determining how robust the pseudo-rigid-body model is for specific mechanisms. The sensitivity of the model with respect to the characteristic radius factor, γ, and the stiffness coefficient, K_Θ, may be an indication of robustness.

5. Improvement in the accuracy of the PRBM by including the relationship between γ and K_Θ and the direction of the reaction forces (n). Both of these PRBM parameters are calculated in terms of n, so instead of using a constant value for each, the force equilibrium equations may be used to solve for the values of γ and K_Θ.

6. Further investigation into the nonlinearities involved in compliant mechanisms and the ability of the PRBM to account for these nonlinearities. This can be studied by additional comparisons between the PRBM and FEA.

7. Inclusion of these analysis methods in software packages that already perform kinematics and static equilibrium. User input to characterize pseudo-body-model relationships would allow greater flexibility.

REFERENCES

Ananthasuresh, G.K., Kota, S., and Gianchandani, Y., 1993, "Systematic Synthesis of Microcompliant Mechanisms - Preliminary Results," *Proceeding of the Third National Applied Mechanisms and Robotics Conference*, Cincinnati, Ohio, Paper No. AMR-93-082.

Bisshopp, K.E., and Drucker, D.C., 1945, "Large Deflection of Cantilever Beams," *Quarterly of Applied Mathematics*, Vol. 3, No. 3, pp. 272-275.

Biswas, A., and Kinzel, G.L., 1998c, "Optimal Tolerance and Clearance Allocation in Mechanisms to Minimize Manufacturing Cost," *Proceedings of the 1998 ASME Design Engineering Technical Conferences*, DETC98/MECH-5940.

Brown, C.T., 1995, "Statistical Models for Position and Profile Variation in Mechanical Assemblies," *M.S. Thesis*, Brigham Young University, Provo, Utah.

Bryzek, J., Petersen, K., and McCulley, W., 1994, "Micromachines on the March," *IEEE Spectrum*, May 1994, pp. 20-31.

Burns, R.H. and Crossley, F.R.E., 1966, "Structural Permutations of Flexible Link Mechanisms," *ASME Paper* No. 66-MECH-5.

Burns, R.H. and Crossley, F.R.E., 1968, "Kinetostatic Synthesis of Flexible Link Mechanisms," *ASME Paper* No. 68-Mech-36.

Chase, K.W., Gao, J., and Magleby, S.P., 1995, "General 2-D Tolerance Analysis of Mechanical Assemblies with Small Kinematic Adjustments," *Journal of Design and Manufacturing*, Vol. 5, pp. 263-274.

Chase, K.W., and Parkinson, A.R., 1991, "A Survey of Research in the Application of Tolerance Analysis to the Design of Mechanical Assemblies," *Research in Engineering Design*, Vol. 3, pp. 23-37.

Choi, J.-H., Lee, S.J., and Choi, D.-H., 1998, "Stochastic Linkage Modeling for Mechanical Error Analysis of Planar Mechanisms," *Mechanics of Structures and Machines*, Vol. 26, No. 3, pp. 257-276.

Cleghorn, W.L., Fenton, R.G., and Fu, J-F, 1993, "Optimum Tolerancing of Planar Mechanisms Based on an Error Sensitivity Analysis", *Transactions of the ASME, Journal of Mechanical Design*, Vol. 115, n 2, pp. 306-313.

Clements, D., 1999, "Implementing Compliant Mechanisms in Micro-Electro Mechanical Systems (MEMS)," M.S. Thesis, Brigham Young University, Provo, Utah.

Coit, W.G., and Riley, D., 1981, "Sensitivity Analysis of the Inverted Slider Crank Straight-Line Generator", *Mechanism and Machine Theory*, Vol. 16, n 4, pp.303-310

Derderian, J.M., 1996, "The Pseudo-Rigid-Body Model Concept and Its Application to Micro Compliant Mechanisms," M.S. Thesis, Brigham Young University, Provo, Utah.

Derderian, J.M., Howell, L.L., Murphy, M.D., Lyon, S.M., and Pack, S.D., 1996, "Compliant Parallel-Guiding Mechanisms," *Proceedings of the 1996 ASME Design Engineering Technical Conferences*, 96-DETC/MECH-1208.

Edwards, B.T., Jensen, B.D., and Howell, L.L., 1999, "A Pseudo-Rigid-Body Model for Functionally Binary Pinned-Pinned Segments Used in Compliant Mechanisms," *Proceedings of the 1999 ASME Design Engineering Technical Conferences*, DETC99/DAC-8644.

Fenton, R.G.., Cleghorn, W.L., and Fu, J.-F., 1989, "Allocation of Dimensional Tolerances for Multiple Loop Planar Mechanisms," *Journal of Mechanisms, Transmissions, and Automation in Design*, Vol. 111, pp. 465-470.

Frecker, M.I., Kota, S., and Kikuchi, N., 1996, "Optimal Synthesis of Compliant Mechanisms to Satisfy Kinematic and Structural Requirements - Preliminary Results," *Proceedings of the 1996 ASME Design Engineering Technical Conferences*, 96-DETC/DAC-1497.

Frecker, M.I., Kota, S., and Kikuchi, N., 1997, "Use of Penalty Function in Topological Synthesis and Optimization of Strain Energy Density of Compliant Mechanisms," *Proceeding of the 1997 ASME Design Engineering Technical Conferences*, DETC97/DAC-3760.

Frecker, M.I., Kikuchi, N., and Kota, S., 1998, "Optimal Design of Compliant Mechanisms for Smart Structures Applications," *Proceedings of the SPIE Conference on Mathematics and Control in Smart Structures*, San Diego, California, Vol. 3323, pp. 234-242.

Fujita, H., 1997, "A Decade of MEMS and Its Future," *Proceedings of IEEE Micro Electro Mechanical Systems*, pp. 1-8.

Gandhi, M.V., and Thompson, B.S., 1981, "The Finite Element Analysis of Flexible Components of Mechanical Systems Using a Mixed Variational Principle," *ASME Design Engineering Technical Conference*, September 28-October 1, Beverly Hills, CA, pp.1-9.

Gao, J., Chase, K.W., and Magleby, S.P., 1995, "Comparison of Assembly Tolerance Analysis by the Direct Linearization and Modified Monte Carlo Simulation Methods," *Proceedings of the ASME Design Engineering Technical Conferences*, DE-Vol. 82, pp. 353-360.

Garrett, R.E. and Hall, A.S., 1969, "Effect of Tolerance and Clearance in Linkage Design," *ASME Journal of Engineering for Industry*, pp. 198-202.

Gorski, W., 1976, "A Review of Literature and a Bibliography on Finite Elastic Deflections of Bars," *Transactions of the Institution of Engineers*, Australia, Civil Engineering Transactions, Vol. 18, No.2, pp. 74-85.

Hartenberg, R.S., and Denavit, J., 1964, *Kinematic Synthesis of Linkages*, McGraw-Hill.

Howell, L.L., and Midha, A., 1994a, "A Method for the Design of Compliant Mechanisms with Small-Length Flexural Pivots," *ASME Journal of Mechanical Design*, Vol. 116, No. 1, pp. 280-290.

Howell, L.L., and Midha A., 1994b, "The Development of Force-Deflection Relationships for Compliant Mechanisms," *Machine Elements and Machine Dynamics, Proceedings of the 1994 ASME Design Technical Conferences*, DE-Vol. 71 part 2, pp. 501-508.

Howell, L.L., and Midha, A., 1995a, "Determination of the Degrees of Freedom of Compliant Mechanisms Using the Pseudo-Rigid-Body Model Concept," *Proceedings of the Ninth World Congress on the Theory of Machines and Mechanisms*, Milano, Italy, Vol. 2, p. 1537-1541.

Howell, L.L., and Midha, A., 1995b, "Parametric Deflection Approximations for End-Loaded, Large-Deflection Beams in Compliant Mechanisms," *ASME Journal of Mechanical Design*, Vol. 117, No. 1, pp. 156-165.

Howell, L.L., and Midha, A., 1996a, "A Loop-Closure Theory for the Analysis and Synthesis of Compliant Mechanisms," *ASME Journal of Mechanical Design*, Vol. 118, No. 1, pp. 121-125.

Howell, L.L., Midha, A., and Murphy, M.D., 1994c, "Dimensional Synthesis of Compliant Constant-Force Slider Mechanisms," *Machine Elements and Machine Dynamics, Design Technical Conference*, Minneapolis, Minnesota, Sept. 12-14, DE-Vol. 71, pp. 509-515.

Howell, L.L., Midha, A., and Norton, T.W., 1996, "Evaluation of Equivalent Spring Stiffness for Use in a Pseudo-Rigid-Body Model of Large-Deflection Compliant Mechanisms," *ASME Journal of Mechanical Design*, Vol. 118, No. 1, pp. 126-131.

Howell, L. L., Rao, S. S., and Midha, A., 1994d, "Reliability-Based Optimal Design of a Bistable Compliant Mechanism," *ASME Journal of Mechanical Design*, December, Vol. 116, No. 1, pp. 1115-1121.

Jensen, B.D., Howell, L.L., Gunyan, D.B., and Salmon, L.G., 1997, "The Design and Analysis of Compliant MEMS Using the Pseudo-Rigid-Body Model," *Microelectromechanical Systems (MEMS) 1997, ASME International Mechanical Engineering Congress and Exposition*, November 16-21, 1997, Dallas, TX, DSC-Vol. 62, pp. 119-126.

Jensen, B.D., Howell, L.L., and Salmon, L.G., 1998, "Introduction of Two-Link In-Plane, Bistable Compliant MEMS," *Proceeding of the 1998 ASME Design Engineering Technical Conferences*, DETC98/MECH-5837.

Joskowicz, L., Sacks, E., and Srinivasan, V., 1997, "Kinematic Tolerance Analysis," *Computer Aided Design*, Vol. 29, No. 2, pp. 147-157.

Koester, D.A., Mahadevan, R., Hardy, B., and Markus, K.W., 2000, *MUMPs™ Design Handbook*, Rev 5.0, Cronos Integrated Microsystems, http://www.memsrus.com/cronos/svcsrules.html.

Kinzel, G.L., and Hall, A.S., 1975, "Tolerances and Clearances in Instrumented Spatial Chains," *Proceedings of the Fourth World Congress on the Theory of Machines and Mechanisms*, Sep 8-12, pp. 185-191.

Knappe, L.F., 1963, "A Technique for Analyzing Mechanism Tolerances," *Machine Design*, April 25, pp. 155-157.

Komvopoulos, K., 1998 "Challenging Issues in Microelectromechanical Systems," *Proceedings of the 1998 ASME International Mechanical Engineering Congress and Exposition, Microelectromechanical Systems (MEMS)*, DSC-Vol. 66, pp. 261-264.

Kota, S., Ananthasuresh, G.K., Crary, S.B., and Wise, K.D., 1994, "Design and Fabrication of Microelectromechanical Systems," *ASME Journal of Mechanical Design*, Vol. 116, pp. 1081-1088.

Lee, S.J., and Gilmore, B.J., 1991, "The Determination of the Probabilistic Properties of Velocities and Accelerations in Kinematic Chains With Uncertainty," *ASME Journal of Mechanical Design*, Vol. 113, pp. 84-90.

Lyon, S.M., Evans, M.S., Erickson, P.A., and Howell, L.L., 1997, "Dynamic Response of Compliant Mechanisms Using the Pseudo-Rigid-Body Model," *Proceedings of the 1997 ASME Design Engineering Technical Conferences*, DETC97/VIB-4177.

Lyon, S.M., Howell, L. L., and Roach, G.M., 2000, "Modeling Flexible Segments with Force and Moment End Loads via the Pseudo-Rigid-Body Model," *Proceedings of the ASME International Mechanical Engineering Congress and Exposition*, Nov. 2000.

Marler, J., 1988, “Nonlinear Tolerance Analysis Using the Direct Linearization Method,” ADCATS Report No. 88-6, Brigham Young University.

Mettlach, G.A., and Midha, A., 1996, "Using Burmester Theory in the Design of Compliant Mechanisms," *Proceedings of the 1996 ASME Design Engineering Technical Conferences*, 96-DETC/MECH-1181.

Millar, A.J., Howell, L.L, and Leonard, J.N., 1996, "Design and Evaluation of Compliant Constant-Force Mechanisms," *Proceedings of the 1996 ASME Design Engineering Technical Conferences and Computers in Engineering Conference*, 96-DETC/MECH-1209.

Mirfendereski, D., Lin, L., Kiureghian, A.D., and Pisano, A.P., 1993, "Probabilistic Response of Micro-Fabricated Polysilicon Beam Structures: Comparison of Analysis and Experiments," *ASME, Dynamic Systems and Control Division*, Vol. 46, pp. 77-80.

Morrisson, P. and Morrisson, E., 1961, "Charles Babbage and his Calculating Engines," Dover Publications Inc., New York.

Opdahl, P.G., 1996, "Modeling and Analysis of Compliant Bi-Stable Mechanisms Using the Pseudo-Rigid-Body Model,” M.S. Thesis, Brigham Young University, Provo, Utah.

Opdahl, P., Jensen, B.D., and Howell, L.L., 1998, "An Investigation into Compliant Bistable Mechanisms,” *Proceedings of the 1998 ASME Design Engineering Technical Conferences*, DETC09/DAC-3763.

Petersen, K.E., 1982, "Silicon as a Mechanical Material," *Proceedings of the IEEE*, Vol. 70, No. 5, May, pp. 420-457.

Rhyu, J.H., and Kwak, B.M., 1988, "Optimal Stochastic Design of Four-Bar Mechanisms for Tolerance and Clearance," *ASME Journal of Mechanisms, Transmissions, and Automation in Design*, Vol. 110, No. 3, pp. 255-262.

Salmon, L.G., Gunyan, D.B., Derderian, J.M., Opdahl, P.G., and Howell, L.L., 1996, "Use of the Pseudo-Rigid-Body Model to Simplify the Description of Compliant Micro Mechanisms," *IEEE Solid-State Sensor and Actuator Workshop, Hilton Head Island,* South Carolina, pp. 136-139.

Schade, G.R., 1983, "A Bivariate Normal Model of Mechanism Coupler-Point Position," *Journal of Mechanisms, Transmissions, and Automation in Design,* Vol. 105, No. 3, pp. 599-605.

Schade, G.R., and Lai, S.-C., 1983, "Effects of Bearing Clearance on Coupler-Point Position," *Proceedings of the Eighth Oklahoma State University Applied Mechanisms Conference*, Sep 19-21, pp. 76:1-5.

Sevak, N.M., and McLarnan, C.W., 1974, "Optimal Synthesis of Flexible Link Mechanisms with Large Static Deflections," *ASME Paper* No. 74-DET-83.

Sharpe, W.N., Yuah, B., Vaidyanathan, R., and Edwards, R.L., 1997, "Measurements of Young's Modulus, Poisson's Ratio and Tensile Strength of Polysilicon," *IEEE Micro-Electro-Mechanical Systems,* pp. 424-429.

Sharpe, W.N., Turner, K.T., and Edwards, R.L., 1999, "Tensile Testing of Polysilicon," *Experimental Mechanics,* Vol. 39, No. 3, pp. 162-170.

Sharpe, W.N., Jr., and Jackson, K., 2000, "Tensile Testing of MEMS Materials," *Presented at SEM 2000, June 5-8, and to be published in the Proceedings,* http://www.me.jhu.edu/~sharpe.

Shi, Z., 1997, "Synthesis of Mechanical Error in Spatial Linkages Based on Reliability Concept," *Mechanism and Machine Theory,* Vol. 32, No. 2, pp. 255-259.

Vocaturo, J.M., 1983, "Evaluating the Repeatability of Linkages," *Machine Design,* June 23, pp. 67-71.

Waldron, K.J., and Kumar, A., 1979, "Development of a Theory of Errors for Manipulators," *Proc. of the 5th World Congress on Theory of Machines and Mechanisms,* pp. 821-826.

Wei-Liang, X., and Qi-Xian, Z., 1989, "Probabilistic Analysis and Monte Carlo Simulation of the Kinematic Error in a Spatial Linkage," *Mechanism and Machine Theory,* Vol. 24, No. 1, pp. 19-27.

Wise, K.D., 1991, "Integrated Microelectromechanical Systems: A Perspective on MEMS in the 90s," *Proceedings of the IEEE Microelectromechanical Systems Workshop,* pp. 33-38.

Wolf, S., and Tauber, R., 2000, *Silicon Processing for the VLSI Era, Volume 1: Process Technology,* 2nd Ed., Lattice Press, Sunset Beach, California.

Yeh, R., and Pister, K.S.J., 1995, "Measurement of Static Friction in Mechanical Couplings of Articulated Microrobots," *SPIE Micromachined Devices and Components,* Vol. 2642, pp. 40-50.

Yin, Z.W., and Wu, J.K., 1990, "An Optimal Synthesis of Linkages Considering Structural Error and Clearances," *Mechanism Synthesis and Analysis, 21st. Biennial Mechanisms Conference,* Sep 16-19, pp. 295-299.

Zhu, J., and Ting, K.-L., 2000, "Uncertainty Analysis of Planar and Spatial Robots with Joint Clearances," *Mechanism and Machine Theory,* Vol. 35, No. 9, pp. 1239-1256.

APPENDIX A

SOLUTION TO EXAMPLE PROBLEM IN CHAPTER 4

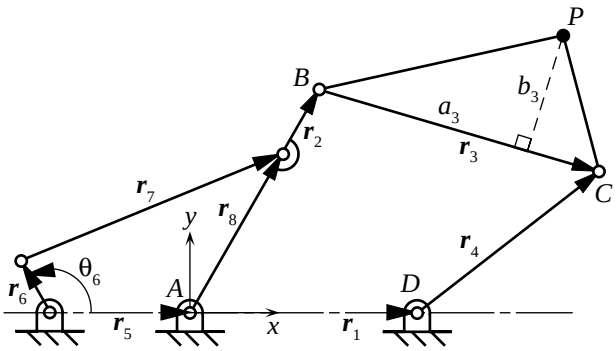

r_1 = 2.36 cm $r_2 = \overrightarrow{AB}$ = 1.33 cm r_3 = 5.08 cm r_4 = 3.94 cm

r_4 = 3.94 cm r_5 = 1.00 cm r_6 = 0.45 cm r_7 = 1.50 cm

r_8 = 1.00 cm a_3 = 6.00 cm b_3 = 0.50 cm

Figure A.1Double-rocker four-bar mechanism with driving crank.

The following are the loop equations that describe this model:

$$h_1() = r_2\cos\theta_2 + r_3\cos\theta_3 - r_4\cos\theta_4 - r_1 = 0$$

$$h_2() = r_2\sin\theta_2 + r_3\sin\theta_3 - r_4\sin\theta_4 = 0$$

$$h_3() = r_6\cos\theta_6 + r_7\cos\theta_7 - r_8\cos\theta_2 - r_5 = 0$$

$$h_4() = r_6\sin\theta_6 + r_7\sin\theta_7 - r_8\sin\theta_2 = 0$$

The following are the matrices used to calculate the final sensitivity matrix for the mechanism used as an example in this paper:

Independent Variable Vector: $[X] = \{r_1, r_2, r_3, r_4, r_5, r_6, r_7, r_8, a_3, b_3\}$

Dependent Variable Vector: $[U] = \{\theta_2, \theta_3, \theta_4, \theta_7\}$

Matrices Used to Determine Sensitivities:

$[A] = (\partial h_i)/(\partial X_j) =$

$$\begin{bmatrix} \frac{\partial h_1}{\partial r_1} & \frac{\partial h_1}{\partial r_2} & \frac{\partial h_1}{\partial r_3} & \frac{\partial h_1}{\partial r_4} & \frac{\partial h_1}{\partial r_5} & \frac{\partial h_1}{\partial r_6} & \frac{\partial h_1}{\partial r_7} & \frac{\partial h_1}{\partial r_8} & \frac{\partial h_1}{\partial a_3} & \frac{\partial h_1}{\partial b_3} \\ \frac{\partial h_2}{\partial r_1} & \frac{\partial h_2}{\partial r_2} & \frac{\partial h_2}{\partial r_3} & \frac{\partial h_2}{\partial r_4} & \frac{\partial h_2}{\partial r_5} & \frac{\partial h_2}{\partial r_6} & \frac{\partial h_2}{\partial r_7} & \frac{\partial h_2}{\partial r_8} & \frac{\partial h_2}{\partial a_3} & \frac{\partial h_2}{\partial b_3} \\ \frac{\partial h_3}{\partial r_1} & \frac{\partial h_3}{\partial r_2} & \frac{\partial h_3}{\partial r_3} & \frac{\partial h_3}{\partial r_4} & \frac{\partial h_3}{\partial r_5} & \frac{\partial h_3}{\partial r_6} & \frac{\partial h_3}{\partial r_7} & \frac{\partial h_3}{\partial r_8} & \frac{\partial h_3}{\partial a_3} & \frac{\partial h_3}{\partial b_3} \\ \frac{\partial h_4}{\partial r_1} & \frac{\partial h_4}{\partial r_2} & \frac{\partial h_4}{\partial r_3} & \frac{\partial h_4}{\partial r_4} & \frac{\partial h_4}{\partial r_5} & \frac{\partial h_4}{\partial r_6} & \frac{\partial h_4}{\partial r_7} & \frac{\partial h_4}{\partial r_8} & \frac{\partial h_4}{\partial a_3} & \frac{\partial h_4}{\partial b_3} \end{bmatrix} =$$

$$\begin{bmatrix} -1 & \cos\theta_2 & \cos\theta_3 & -\cos\theta_4 & 0 & 0 & 0 & 0 & 0 & 0 \\ 0 & \sin\theta_2 & \sin\theta_3 & -\sin\theta_4 & 0 & 0 & 0 & 0 & 0 & 0 \\ 0 & 0 & 0 & 0 & -1 & \cos\theta_6 & \cos\theta_7 & -\cos\theta_2 & 0 & 0 \\ 0 & 0 & 0 & 0 & 0 & \sin\theta_6 & \sin\theta_7 & -\sin\theta_2 & 0 & 0 \end{bmatrix}$$

$$[B] = (\partial h_i)/(\partial U_j) =$$

$$\begin{bmatrix} \frac{\partial h_1}{\partial \theta_2} & \frac{\partial h_1}{\partial \theta_3} & \frac{\partial h_1}{\partial \theta_4} & \frac{\partial h_1}{\partial \theta_7} \\ \frac{\partial h_2}{\partial \theta_2} & \frac{\partial h_2}{\partial \theta_3} & \frac{\partial h_2}{\partial \theta_4} & \frac{\partial h_2}{\partial \theta_7} \\ \frac{\partial h_3}{\partial \theta_2} & \frac{\partial h_3}{\partial \theta_3} & \frac{\partial h_3}{\partial \theta_4} & \frac{\partial h_3}{\partial \theta_7} \\ \frac{\partial h_4}{\partial \theta_2} & \frac{\partial h_4}{\partial \theta_3} & \frac{\partial h_4}{\partial \theta_4} & \frac{\partial h_4}{\partial \theta_7} \end{bmatrix} = \begin{bmatrix} -r_2\sin\theta_2 & -r_3\sin\theta_3 & r_4\sin\theta_4 & 0 \\ r_2\cos\theta_2 & r_3\cos\theta_3 & -r_4\cos\theta_4 & 0 \\ r_8\sin\theta_2 & 0 & 0 & -r_7\sin\theta_7 \\ -r_8\cos\theta_2 & 0 & 0 & r_7\cos\theta_7 \end{bmatrix}$$

$$[C] = (\partial P_i)/(\partial X_j) =$$

$$\begin{bmatrix} \frac{\partial P_x}{\partial r_1} & \frac{\partial P_x}{\partial r_2} & \frac{\partial P_x}{\partial r_3} & \frac{\partial P_x}{\partial r_4} & \frac{\partial P_x}{\partial r_5} & \frac{\partial P_x}{\partial r_6} & \frac{\partial P_x}{\partial r_7} & \frac{\partial P_x}{\partial r_8} & \frac{\partial P_x}{\partial a_3} & \frac{\partial P_x}{\partial b_3} \\ \frac{\partial P_y}{\partial r_1} & \frac{\partial P_y}{\partial r_2} & \frac{\partial P_y}{\partial r_3} & \frac{\partial P_y}{\partial r_4} & \frac{\partial P_y}{\partial r_5} & \frac{\partial P_y}{\partial r_6} & \frac{\partial P_y}{\partial r_7} & \frac{\partial P_y}{\partial r_8} & \frac{\partial P_y}{\partial a_3} & \frac{\partial P_y}{\partial b_3} \end{bmatrix} =$$

$$\begin{bmatrix} 0 & \cos\theta_2 & 0 & 0 & 0 & 0 & 0 & 0 & \cos\theta_3 & \cos(\theta_3+90) \\ 0 & \sin\theta_2 & 0 & 0 & 0 & 0 & 0 & 0 & \sin\theta_3 & \sin(\theta_3+90) \end{bmatrix}$$

$$[D] = (\partial P_i)/(\partial U_j) =$$

$$\begin{bmatrix} \frac{\partial P_x}{\partial \theta_2} & \frac{\partial P_x}{\partial \theta_3} & \frac{\partial P_x}{\partial \theta_4} & \frac{\partial P_x}{\partial \theta_7} \\ \frac{\partial P_y}{\partial \theta_2} & \frac{\partial P_y}{\partial \theta_3} & \frac{\partial P_y}{\partial \theta_4} & \frac{\partial P_y}{\partial \theta_7} \end{bmatrix} = \begin{bmatrix} -r_2\sin\theta_2 & (-a_3\sin\theta_3 - b_3\sin(\theta_3+90)) & 0 & 0 \\ r_2\cos\theta_2 & (a_3\cos\theta_3 + b_3\cos(\theta_3+90)) & 0 & 0 \end{bmatrix}$$

For an input crank angle of 120 degrees, the following sensitivity matrix is obtained:

$$[S] = [C - EB^{-1}A] =$$

$$\begin{bmatrix} -0.641 & 0.936 & 0.826 & -0.947 & -3.616 & -0.444 & 3.944 & -2.100 & 0.950 & -0.312 \\ 1.512 & -0.866 & -1.951 & 2.235 & 3.332 & 0.409 & -3.634 & 1.935 & 0.312 & 0.950 \end{bmatrix}$$

APPENDIX B

BATCH FILE FOR FINITE ELEMENT MODEL

```
!INPUT FILE FOR ANSYS (R)
!Filename: ParallelMech.inp
!Date: June 15, 2001

!**************BEGIN PREPROCESSOR STEPS******************
/TITLE,Analysis of Compliant Young Mechanism
/PREP7

!**************SET UP MODEL VARIABLES********************
R1=200               !*** Link 1 length
L2=200               !*** Link 2 length
Theta2o=90           !*** Initial Angle of link 2 (Degrees)
L3=200               !*** Link 3 length
Theta3o=0            !*** Intiial Angle of link 3 (Degrees)
L4=200               !*** Link 4 length
Theta4o=90           !*** Initial Angle of link 4 (Degrees)
La3=100              !*** Length of a3
Lb3=20               !*** Length of b3

!*********Maximum INPUT DISPLACEMENT********
DelXMax=100

!*************VARIATION/TOLERANCES***************
VarR1=0
VarL2=0
VarL3=0
VarL4=0
VarLa3=0
VarLb3=0
```

```
VarH2=0
VarH4=0
VarW2=0
VarW4=0
VarE=0

!************CROSS SECTIONAL DIMENSIONS***********
h2=3+VarH2              !*** height of flexible link 2
h3=40                   !*** height of rigid link 3
h4=3+VarH4              !*** height of flexible link 4
t2=2+VarW2              !*** thickness of flexible link 2
t3=30                   !*** thickness of rigid link 3
t4=2+VarW4              !*** thickness of flexible link 4
Eyoung=162000+VarE      !*** Young's modulus

PI=acos(-1.)

!***Angles in Radians***************
q2o=Theta2o*PI/180
q3o=Theta3o*PI/180
q4o=Theta4o*PI/180

!***ADD VARIATION TO THE LINK LENGTHS*******
R1=R1+VarR1
L2=L2+VarL2
L3=L3+VarL3
L4=L4+VarL4
La3=La3+VarLa3
Lb3=Lb3+VarLb3

!***Coordinates of Key Points************
K1x=0
K1y=0
K2x=(L2)*cos(q2o)
K2y=(L2)*sin(q2o)
K3x=K2x+(L3)*cos(q3o)
K3y=K2y+(L3)*sin(q3o)
K4x=K3x-(L4)*cos(q4o)
K4y=K3y-(L4)*sin(q4o)
K1000x=K2x+(La3)*cos(q3o)+(Lb3)*cos(q3o+PI/2)
K1000y=K2y+(La3)*sin(q3o)+(Lb3)*sin(q3o+PI/2)

!***INITIAL DISPLACEMENT of POINT 4*********
delK4x=K4x-R1
delK4y=K4y
```

```
!***Area Properties
I2=t2*h2*h2*h2/12        !*** Moment of Inertia
I3=t3*h3*h3*h3/12
I4=t4*h4*h4*h4/12
A2=t2*h2                 !*** Cross-Sectional Area
A3=t3*h3
A4=t4*h4

!********** Create the KEY POINTS ************
K,1,K1x,K1y,0
K,2,K2x,K2y,0
K,3,K3x,K3y,0
K,4,K4x,K4y,0
K,5,K5x,K5y,0
K,1000,K1000x,K1000y,0

!********* Create the LINES between the KEYPOINTS *******
L,1,2
LESIZE,1,,,50
L,3,4
LESIZE,2,,,50
l,2,3
LESIZE,3,,,5
l,1,5
LESIZE,4,,,5
l,2,1000
LESIZE,5,,,5
l,3,1000
LESIZE,6,,,5

!***** Display Lines *****
LPLOT
!***** Fit to Screen *****
/AUTO,1

!******* Declare the ELEMENT TYPE: Beam 3 (2D Elastic) *****
ET,1,BEAM3

!************* SET CONSTANTS ****************
!    Set 1: Link 2 (flexible)
!    Set 2: Link 3 (Rigid)
!    Set 3: Link 4 (flexible)
!    Assume no shearz, no prestrain, no mass properties
R,1,A2,I2,h2,0,0,0
```

```
R,2,A3,I3,h3,0,0,0
R,3,A4,I4,h4,0,0,0

!******** Set Material Properties on Material 1 *******
MP,EX,1,Eyoung

!********* MESH: LMESH{NL1,NL2,NINC} or LMESH,ALL
real,1
type,1
mat,1
LMESH,1
real,3
lmesh,2
real,2
lmesh,3,6

!*********GET NODES ASSOCIATED WITH KEY POINTS **********
ksel,s,kp,,5
nslk,s
*get,nkp5,node,0,num,max
nsel,all
ksel,all

ksel,s,kp,,4
nslk,s
*get,nkp4,node,0,num,max
nsel,all
ksel,all

ksel,s,kp,,1000
nslk,s
*get,nkp1000,node,0,num,max
nsel,all
ksel,all

ksel,s,kp,,2
nslk,s
*get,nkp2,node,0,num,max
nsel,all
ksel,all

FINISH

!***************BEGIN SOLUTION STEPS*****************
/SOLU
```

```
!********** Set to Nonlinear Deflection Analysis
NLGEOM,1

!********** Set Analysis Type to Static (0)
ANTYPE,0
!************************ LOAD STEPS *********************
! Constrain Node 1 & 4 in X & Y Directions
DK,1, ,0, , , ,UX,UY, , , ,
DK,4,UX,R1-K4x
DK,4,UY,-K4y
lswrite,1
! INPUT DISPLACEMENT
! Constrain Node 5 in the X direction
DK,1000, ,DelXMax/10, , , ,UX, , , , ,
lswrite,2
DK,1000, ,DelXMax*2/10, , , ,UX, , , , ,
lswrite,3
DK,1000, ,DelXMax*3/10, , , ,UX, , , , ,
lswrite,4
DK,1000, ,DelXMax*4/10, , , ,UX, , , , ,
lswrite,5
DK,1000, ,DelXMax*5/10, , , ,UX, , , , ,
lswrite,6
DK,1000, ,DelXMax*6/10, , , ,UX, , , , ,
lswrite,7
DK,1000, ,DelXMax*7/10, , , ,UX, , , , ,
lswrite,8
DK,1000, ,DelXMax*8/10, , , ,UX, , , , ,
lswrite,9
DK,1000, ,DelXMax*9/10, , , ,UX, , , , ,
lswrite,10
DK,1000, ,DelXMax*10/10, , , ,UX, , , , ,
lswrite,11
lssolve,1,11

FINISH

!*****Store Nodal Solutions ********
/POST26
NSOL,2,nkp1000,U,X,DelP3x
NSOL,3,nkp1000,U,Y,DelP3y
NSOL,4,nkp1000,ROT,Z,DelP3q
RFORCE,5,nkp1000,F,X,FxOut
/output,output
```

```
prvar,2,3,4,5
/output

FINISH

!*************** GET STRESSES and MOMENTS ****************
/POST1
SET,LAST
ETABLE,smxi,NMIS,1
ETABLE,smxj,NMIS,3
ETABLE,smni,NMIS,2
ETABLE,smnj,NMIS,4
ETABLE,mmozi,SMIS,6
ETABLE,mmozj,SMIS,12
FINISH

/eof
```